Theory of noncollinear magnetism in amorphous transition metals

T. Uchida
Hokkaido Institute of Technology, Maeda, Teine-ku, Sapporo 006-8585, Japan

Y. Kakehashi
Max-Planck-Institut für Physik komplexer Systeme, D-01187 Dresden, Germany
and Hokkaido Institute of Technology, Maeda, Teine-ku, Sapporo 006-8585, Japan
(Received 28 November 2000; published 28 June 2001)

The noncollinear magnetism in amorphous transition metals has been investigated by developing the finite-temperature theory of amorphous-metallic magnetism, which takes into account the transverse spin degrees of freedom. The theory is based on the functional-integral technique to the degenerate-band Hubbard Hamiltonian and the distribution function method for local magnetic moments with structural disorder. Numerical results are presented for the magnetic phase diagram as a function of *d* electron number *N* and temperature *T*, and for the magnetization vs volume curves for *d* electron numbers in the vicinity of amorphous Fe. The calculated magnetic phase diagram on the *N*-*T* plane exhibits three ordered phases at low temperatures: the spin glass (SG) in the region $N \leqslant 7.38$, the noncollinear ferromagnetism (*F*) in the region $7.38 \leqslant N \leqslant 7.43$, and the collinear *F* in the region $N \geqslant 7.43$. The noncollinear SG is expected in the region $6.9 < N \leqslant 7.38$, while the SG transition temperatures for the collinear and the noncollinear SG are almost the same for $N \leqslant 6.9$. In the vicinity of the multicritical point on the *N*-*T* plane, the transition from the collinear *F* to the noncollinear *F* is shown to occur with decreasing temperature, due to the freezing of transverse spin components. The result seems to be consistent with those of the recent Mössbauer measurements on Fe-rich amorphous transition-metal alloys. The calculated volume dependence at 35 K shows a clear phase transition from the *F* to the noncollinear SG with decreasing volume, and a subsequent transition to the paramagnetism. The type of the transition from the *F* to SG is found to depend on *N*: the first order for $N = 7.0$, and the second order for $N = 7.3$.

DOI: 10.1103/PhysRevB.64.054402 PACS number(s): 75.10.Lp, 75.10.Nr, 75.50.Bb, 75.50.Kj

I. INTRODUCTION

In the last two decades, the magnetism of amorphous transition metals and their alloys has been a subject of intensive experimental and theoretical research. Experimental investigations on Fe-, Co-, and Ni-rich amorphous transition-metal alloys demonstrated that the magnetic properties of these amorphous systems are quite different from those of the crystalline counterparts.[1–3] In Fe-rich amorphous alloys containing early transition metals, it was found that the Curie temperatures rapidly decrease beyond 85 at.% Fe, and, to our knowledge, a novel phase of spin glass (SG) appears beyond 90 at.% Fe.[4–11] Since the SG transition temperatures hardly depend on the second elements, it was considered that the SG is caused by the structural disorder intrinsic in pure amorphous Fe.

Kakehashi developed a finite-temperature theory of amorphous metallic magnetism[12–14] on the basis of the functional-integral method[15–17] and the distribution function method.[18] The theory explained the SG of amorphous Fe in terms of a competition between the ferro- and the antiferromagnetic interactions due to the nonlinear magnetic couplings between Fe local moments and the local environment effects on the amplitude of the local moments. Subsequently, Yu *et al.* extended the theory to the case of amorphous-metallic alloys and calculated the magnetic phase diagram of amorphous Fe-Zr alloys as a function of Fe concentration and temperature.[19] The theory successfully explained the observed transition from the ferromagnetism (*F*) to the SG with increasing Fe concentration in Fe-rich amorphous Fe-Zr alloys.

On the other hand, most of the experimental data of amorphous Fe, other than those of Fe-rich amorphous transition-metal alloys, were reported to show the ferromagnetism. The amorphous Fe in the Y/Fe/Y sandwich film,[20] for example, was reported to show the ferromagnetism with the ground-state magnetization $1.2\mu_B$. The amorphous Fe powders containing 2 wt. % H, 3 wt. % C, and 1 wt. % O were also reported to show the ferromagnetism with the magnetization $1.4\mu_B$ at the ground state.[21] Therefore, it was controversial whether the pure amorphous Fe shows the SG or the ferromagnetism.

In order to elucidate the origins of the contradictory experimental results mentioned above, the volume dependence of the SG state and the influence of the degree of structural disorder on the magnetic phase diagram were investigated in subsequent papers. In the calculations of the volume dependence, it was found that the equilibrium volume of amorphous Fe is expected to be close to the phase boundary between the ferromagnetism and the SG.[22] It was suggested that the ferromagnetism in the Y/amorphous Fe/Y film might appear due to the volume expansion. To examine the influence of the degree of structural disorder, the theory which interpolates crystals and amorphous structures was developed, and the magnetic phase diagram was calculated as a function of the coordination number and the fluctuation of interatomic distance.[23,24] The phase diagram explained the nonunique magnetism observed in Fe-rich amorphous alloys; the ferromagnetism in the amorphous Fe powder, and the SG in Fe-rich amorphous alloys containing early transition metals.

The magnetic properties of amorphous Fe have also been investigated on the basis of the ground-state theories. At the early stage of investigations, the ground-state calculations for amorphous Fe reported the ferromagnetism.[25–28] Later, the noncollinear ground-state calculations suggested the possibility of the SG in amorphous Fe. Krey *et al.*[29] obtained two self-consistent solutions with magnetization $1.17\mu_B$ and $0.2\mu_B$, which are almost degenerate in energy, using the tight-binding supercell method with 54 atoms. Lorenz *et al.*[30] performed detailed noncollinear calculations based on the self-consistent linear muffin-tin orbital (LMTO) recursion method with 1728 atoms in a cluster, and found that the ground-state magnetization decreases up to $0.5\mu_B$ with the SG-like random local moment configuration. More recent noncollinear calculations by Liebs *et al.*[31] with use of the LMTO supercell method with 32 Fe atoms in a unit cell, showed that the SG can become the ground state for amorphous Fe.

In spite of the fact that the theoretical efforts mentioned above brought much understanding on the magnetism of amorphous Fe and Fe-rich amorphous alloys, there have been no theoretical attempts, so far, to investigate the noncollinear magnetism of amorphous metals at finite temperatures. Thus, for example, the magnetic phase diagram of amorphous transition metals, including noncollinear magnetism, has not been clarified yet theoretically. The experiments on Fe-rich alloys also show the necessity of the noncollinear finite-temperature theory. The recent Mössbauer[8,32–34] and neutron-diffraction measurements[35] have yielded much evidence for noncollinear magnetism in Fe-rich amorphous alloys. In particular, an issue of interest in Fe-rich amorphous transition-metal alloys has been the experimental observation that the noncollinear state appears at a temperature below the Curie temperature T_C, due to the spin freezing.[5,6,8,32–34,36] It was found experimentally that the obtained magnetic phase diagram[4] as a function of the Fe concentration and temperature is similar to the one obtained in the mean-field theory of the random bond classical Heisenberg model by Gabay and Toulouse.[37] Recently, the detailed Monte Carlo calculations on the basis of the random bond Heisenberg model[38] have been performed to explain the spin freezing phenomenon. The spin freezing in Fe-rich amorphous alloys, however, should be explained on the basis of the itinerant model, since the Fe-rich amorphous alloys show the characteristic features of itinerant magnetism, such as the amplitude fluctuations of local magnetic moments at low temperatures.[8]

The purpose of the present paper is first to develop a finite-temperature theory of noncollinear magnetism, which describes qualitatively or semiquantitatively the magnetic properties of amorphous transition metals starting from the itinerant model, and then to investigate the unraveled problems in amorphous transition metals, specifically those regarding amorphous Fe: the spin glass due to the structural disorder, the transverse spin freezing phenomenon, and the volume dependence of the noncollinear magnetism.

In the following section, we formulate the noncollinear theory of amorphous-metallic magnetism on the basis of the functional-integral method and the distribution function method. In order to take into account the transverse spin degrees of freedom at finite temperatures, we derive the free energy that reduces to the generalized Hartree-Fock approximation at the ground state using the two-field static approximation.[17]

In Sec. III A, we present the numerical results for amorphous transition metals as a function of the *d* electron number N and the temperature T. The present results yield the noncollinear SG due to the structural disorder at low temperatures after disappearance of the ferromagnetism with decreasing the *d* electron number, supporting the existence of SG in amorphous Fe. This is consistent with the experimental observations[4] on Fe-rich amorphous transition metal alloys. Furthermore, we show that the transverse spin freezing occurs below the Curie temperature with the decrease of temperature as well as with the decrease of the *d* electron number, yielding the magnetic phase diagram consisting of four phases: the collinear ferromagnetism, the noncollinear ferromagnetism, the spin glass, and the paramagnetism. The result explains the recent Mössbauer experiments[8,32–34] on Fe-rich amorphous transition-metal alloys. The results of preliminary calculations for this part have been published as the proceedings.[39–41]

In Sec. III B, the numerical results for the volume dependence in the vicinity of amorphous Fe are presented. The previous ground-state calculations for amorphous Fe[30] showed a gradual decrease of magnetization towards the SG-like state with compression, yielding no signs of a clear phase transition, in disagreement with the results of the finite-temperature theory for collinear local moments.[22] We found a clear phase transition from the ferromagnetism to the noncollinear SG and a subsequent transition to the paramagnetism with decreasing volume in agreement with the experiments on Fe-rich amorphous transition-metal alloys under pressure.[42] In Sec. IV, we summarize the present results and discuss the remaining problems.

II. FORMULATION

A. Functional-integral technique

In order to describe the itinerant electron magnetism in the amorphous-metallic system, we start from the *D*-fold degenerate-band Hamiltonian with the intra-atomic Coulomb (U_i) and exchange (J_i) interactions:

$$H = H_0 + H_1, \tag{1}$$

$$H_0 = \sum_{i\nu\sigma} (\epsilon_i^0 - h_i\sigma) n_{i\nu\sigma} + \sum_{i\nu j\nu'\sigma} t_{ij} a_{i\nu\sigma}^\dagger a_{j\nu'\sigma}, \tag{2}$$

$$H_1 = \frac{1}{4} \sum_i U_i n_i^2 - \sum_i J_i \boldsymbol{S}_i^2 . \tag{3}$$

Here ϵ_i^0 and t_{ij}, in the one-electron part H_0, are the atomic level on site i and the transfer integral between the sites i and j, respectively. h_i is the external magnetic field on site i. $a_{i\nu\sigma}^\dagger (a_{i\nu\sigma})$ is the creation (annihilation) operator for an electron with spin σ and orbital ν on site i, and $n_{i\nu\sigma} = a_{i\nu\sigma}^\dagger a_{i\nu\sigma}$ is the number operator for the electrons on site i

with orbital ν and spin σ. Furthermore, n_i and $\boldsymbol{S}_i$ in the interaction part H_1, denote the charge and spin density operators on site i, which are defined by $n_i=\Sigma_{\nu\sigma}n_{i\nu\sigma}$ and $\boldsymbol{S}_i=\Sigma_{\nu\sigma\sigma'}a^{\dagger}_{i\nu\sigma}(\boldsymbol{\sigma})_{\sigma\sigma'}a_{i\nu\sigma'}/2$, $\boldsymbol{\sigma}$, the Pauli spin matrices, respectively.

We apply the functional-integral method to the Hamiltonian (1), which transforms the interacting-electron system to a one-electron system with the time-dependent charge and exchange fields.[43,44] The method, however, gives different results, depending on the form of the interaction part H_1, when we adopt the static approximation in which the time dependence of the fields is neglected.[17] In order to describe best the noncollinear magnetism within the static approximation, we follow the conventional method leading to the generalized Hartree-Fock approximation at the ground state in the present section.

We first introduce the locally rotated coordinates at each site, and rewrite the interacting Hamiltonian (3) in terms of the operators on the rotated coordinates:

$$H_1=-\sum_i\sum_{\nu\nu'}\left(-\frac{1}{4}\hat{n}_{i\nu}A_{i\nu\nu'}\hat{n}_{i\nu'}+\frac{1}{4}\sum_{\alpha}^{\mathbf{x},\mathbf{y},\mathbf{z}}\hat{m}_{i\nu\alpha}B^{\alpha}_{i\nu\nu'}\hat{m}_{i\nu'\alpha}\right), \tag{4}$$

where

$$A_{i\nu\nu'}=\frac{1}{2}(U_i+3J_i)\delta_{\nu\nu'}+U_i(1-\delta_{\nu\nu'}), \tag{5}$$

$$B^{\alpha}_{i\nu\nu'}=J_i(1-\delta_{\nu\nu'})\quad(\alpha=\mathbf{x},\mathbf{y}), \tag{6}$$

$$B^{\mathbf{z}}_{i\nu\nu'}=\frac{1}{2}(U_i+3J_i)\delta_{\nu\nu'}+J_i(1-\delta_{\nu\nu'}). \tag{7}$$

Here the hats on the operators indicate that those operators are defined on the rotated coordinates: $\hat{n}_{i\nu}=\Sigma_{\sigma}\hat{a}^{\dagger}_{i\nu\sigma}\hat{a}_{i\nu\sigma}$ and $\hat{m}_{i\nu\alpha}=\Sigma_{\sigma\sigma'}\hat{a}^{\dagger}_{i\nu\sigma}(\sigma_{\alpha})_{\sigma\sigma'}\hat{a}_{i\nu\sigma'}$. The creation (annihilation) operators $\hat{a}^{\dagger}_{i\nu\sigma}$ ($\hat{a}_{i\nu\sigma}$) for an electron with spin σ, which is quantized along the $\mathbf{z}$ axis of the rotated coordinates on site i, are given by

$$\hat{a}^{\dagger}_{i\nu\sigma}=\sum_{\sigma'}a^{\dagger}_{i\nu\sigma'}D_{\sigma'\sigma}(R_i), \tag{8}$$

$$\hat{a}_{i\nu\sigma}=\sum_{\sigma'}a_{i\nu\sigma'}D^{*}_{\sigma'\sigma}(R_i), \tag{9}$$

where $D_{\sigma\sigma'}(R_i)$ is a rotation matrix for a spin on site i defined by

$$D(R_i)=\begin{pmatrix}\cos\frac{\theta_i}{2}e^{-i(\phi_i/2)} & -\sin\frac{\theta_i}{2}e^{-i(\phi_i/2)}\\ \sin\frac{\theta_i}{2}e^{i(\phi_i/2)} & \cos\frac{\theta_i}{2}e^{i(\phi_i/2)}\end{pmatrix}. \tag{10}$$

Here θ_i and ϕ_i denote the zenith and azimuth angles of the $\mathbf{z}$ axis in the rotated coordinates on site i.

The partition function Z leading to the free energy at temperature T is given by

$$Z=\mathrm{Tr}\left[\mathcal{T}\exp\left(-\int_0^{\beta}H(\tau)d\tau\right)\right]. \tag{11}$$

Here $\mathcal{T}$ denotes the time-ordered product, and β denotes the inverse temperature: $\beta=1/k_{\mathrm{B}}T$. $H(\tau)$ is the Hamiltonian in the interaction representation defined by

$$H(\tau)=e^{\tau K_0}He^{-\tau K_0}, \tag{12}$$

$$K_0=H_0-\mu N_{\mathrm{e}}, \tag{13}$$

where μ and N_{e} denote the chemical potential and the total number of electrons, respectively.

We next adopt the functional-integral technique to the Hamiltonian on the rotated coordinates. The method transforms under the $\mathcal{T}$ product the interacting Hamiltonian (4) into the one-electron Hamiltonian with time-dependent random charge and exchange fields $\{\zeta_{i\nu}(\tau),\boldsymbol{\xi}_{i\nu}(\tau)\}$ by means of the Hubbard-Stratonovich transformation:[43,44]

$$\begin{aligned}e^{-H_1(\tau)\Delta\tau}=&\left[\prod_{i=1}^{N_{\mathrm{s}}}\left(\frac{(\Delta\tau)^D\det A_i}{(4\pi)^D}\prod_{\alpha}^{\mathbf{x},\mathbf{y},\mathbf{z}}\frac{(\Delta\tau)^D\det B^{\alpha}_i}{(4\pi)^D}\right)^{1/2}\right]\int\left[\prod_{i=1}^{N_{\mathrm{s}}}\prod_{\nu=1}^{D}d\boldsymbol{\xi}_{i\nu}(\tau)d\zeta_{i\nu}(\tau)\right]\\&\times\exp\left[-\frac{\Delta\tau}{4}\sum_{i\nu\nu'}\left(\zeta_{i\nu}(\tau)A_{i\nu\nu'}\zeta_{i\nu'}(\tau)+\sum_{\alpha}^{\mathbf{x},\mathbf{y},\mathbf{z}}\xi_{i\nu\alpha}(\tau)B^{\alpha}_{i\nu\nu'}\xi_{i\nu'\alpha}(\tau)\right)\right.\\&\left.+\frac{\Delta\tau}{2}\sum_{i\nu\nu'}\left(i\zeta_{i\nu}(\tau)A_{i\nu\nu'}\hat{n}_{i\nu'}(\tau)+\sum_{\alpha}^{\mathbf{x},\mathbf{y},\mathbf{z}}\xi_{i\nu\alpha}(\tau)B^{\alpha}_{i\nu\nu'}\hat{m}_{i\nu'\alpha}(\tau)\right)\right].\end{aligned} \tag{14}$$

Here $\Delta\tau$ is an infinitesimal time interval. N_{s} denotes the number of sites, D denotes the orbital degeneracy, and $\det A_i$ denotes the determinant of matrix $A_{i\nu\nu'}$ for orbital indices.

The partition function (11) is then written as

$$Z=\int\left[\prod_{i=1}^{N_s}\prod_{\nu=1}^{D}\delta\boldsymbol{\xi}_{i\nu}(\tau)\,\delta\zeta_{i\nu}(\tau)\right]Z^0[\boldsymbol{\xi}(\tau),\zeta(\tau)]$$
$$\times\exp\left[-\frac{1}{4}\sum_{i\nu\nu'}\int_0^\beta d\tau\left(\zeta_{i\nu}(\tau)A_{i\nu\nu'}\zeta_{i\nu'}(\tau)+\sum_{\alpha}^{\mathbf{x},\mathbf{y},\mathbf{z}}\xi_{i\nu\alpha}(\tau)B^{\alpha}_{i\nu\nu'}\xi_{i\nu'\alpha}(\tau)\right)\right], \tag{15}$$

where

$$Z^0[\boldsymbol{\xi}(\tau),\zeta(\tau)]=\mathrm{Tr}\left[\mathcal{T}\exp\left(-\int_0^\beta H[\tau,\boldsymbol{\xi}(\tau),-i\zeta(\tau)]d\tau\right)\right], \tag{16}$$

and

$$H[\tau,\boldsymbol{\xi}(\tau),-i\zeta(\tau)]=K_0(\tau)-\frac{1}{2}\sum_{i\nu\nu'}\left(i\zeta_{i\nu}(\tau)A_{i\nu\nu'}\hat{n}_{i\nu'}(\tau)+\sum_{\alpha}^{\mathbf{x},\mathbf{y},\mathbf{z}}\xi_{i\nu\alpha}(\tau)B^{\alpha}_{i\nu\nu'}\hat{m}_{i\nu'\alpha}(\tau)\right). \tag{17}$$

Here the functional integrals are defined as

$$\int\prod_{n=1}^{N'}\left[\left(\frac{(\Delta\tau)^D\ \det A_i}{(4\pi)^D}\right)^{1/2}\prod_{\nu=1}^{D}d\zeta_{i\nu}(\tau_n)\right]\rightarrow\int\left[\prod_{\nu=1}^{D}\delta\zeta_{i\nu}(\tau)\right], \tag{18}$$

$$\int\prod_{n=1}^{N'}\left[\left(\frac{(\Delta\tau)^D\ \det B_i^{\alpha}}{(4\pi)^D}\right)^{1/2}\prod_{\nu=1}^{D}d\xi_{i\nu\alpha}(\tau_n)\right]\rightarrow\int\left[\prod_{\nu=1}^{D}\delta\xi_{i\nu\alpha}(\tau)\right], \tag{19}$$

where the imaginary time τ is divided into N' points in the range $[0,\beta]$, and τ_n denotes the nth point.

It is difficult to perform the integrals in Eq. (15) even for simple crystalline systems. Thus, we adopt the two-field static approximation,[17,45] which allows us to derive the free energy that reduces to the generalized Hartree-Fock approximation at the ground state. In this approximation, we introduce the time-averaged variables such as

$$\zeta_i=\frac{1}{\beta}\int_0^\beta\sum_{\nu=1}^{D}\zeta_{i\nu}(\tau)d\tau, \tag{20}$$

$$\xi_i=\frac{1}{\beta}\int_0^\beta\sum_{\nu=1}^{D}\xi_{i\nu\mathbf{z}}(\tau)d\tau, \tag{21}$$

and project the partition function onto the subspace $\{\zeta_i,\xi_i\}$ by inserting into Eq. (15) the identities such as

$$1=\int d\zeta_i\,\delta\left(\zeta_i-\frac{1}{\beta}\int_0^\beta\sum_{\nu=1}^{D}\zeta_{i\nu}(\tau)d\tau\right)$$
$$=\int d\zeta_i\int dy_i\exp\left[-2\pi i y_i\left(\zeta_i-\frac{1}{\beta}\int_0^\beta\sum_{\nu=1}^{D}\zeta_{i\nu}(\tau)d\tau\right)\right]. \tag{22}$$

The partition function is then given by

$$Z=\int\prod_{i=1}^{N_s}[d\zeta_i\,d\xi_i]X(\xi,\zeta), \tag{23}$$

$$X(\xi,\zeta)=\int\left[\prod_{i=1}^{N_s}\left(\prod_{\nu=1}^{D}\delta\boldsymbol{\xi}_{i\nu}(\tau)\,\delta\zeta_{i\nu}(\tau)\right)dx_i\,dy_i\right]Z^0[\boldsymbol{\xi}(\tau),\zeta(\tau)]$$
$$\times\exp\left[-\frac{1}{4}\sum_{i\nu\nu'}\int_0^\beta d\tau\,\zeta_{i\nu}(\tau)A_{i\nu\nu'}\zeta_{i\nu'}(\tau)+2\pi i\sum_{i\nu}y_i\beta^{-1}\int_0^\beta d\tau[\zeta_{i\nu}(\tau)-\zeta_i/D]\right.$$
$$\left.-\frac{1}{4}\sum_{i\nu\nu'\alpha}\int_0^\beta d\tau\,\xi_{i\nu\alpha}(\tau)B^{\alpha}_{i\nu\nu'}\xi_{i\nu'\alpha}(\tau)+2\pi i\sum_{i\nu}x_i\beta^{-1}\int_0^\beta d\tau[\xi_{i\nu\mathbf{z}}(\tau)-\xi_i/D]\right]. \tag{24}$$

When we approximate the time-dependent field variables on the rotated coordinates $\{\xi_{i\nu\mathbf{x}}(\tau),\xi_{i\nu\mathbf{y}}(\tau),\xi_{i\nu\mathbf{z}}(\tau),\zeta_{i\nu}(\tau)\}$ with the time-independent variables $\{0,0,\xi_i/D,\zeta_i/D\}$ in the one-electron Hamiltonian (17), we can perform the integrations in $X(\xi,\zeta)$. Here we neglected the transverse static spin fluctuations on the rotated coordinates since they would violate the commutation relations between the spins on the same site. The partition function is then given by

$$Z(\{\boldsymbol{e}_i\}) = \int \prod_{i=1}^{N_s} \left[\left(\frac{\beta \tilde{J}_i}{4\pi} \right)^{1/2} d\xi_i \left(\frac{\beta \tilde{U}_i}{4\pi} \right)^{1/2} d\zeta_i \right] \times \mathrm{Tr}\{\exp[-\beta H_{\mathrm{st}}(\xi \boldsymbol{e}, -i\zeta)]\} \times \exp\left[-\frac{1}{4}\beta \sum_i (\tilde{U}_i \zeta_i^2 + \tilde{J}_i \xi_i^2) \right], \tag{25}$$

$$H_{\mathrm{st}}(\xi \boldsymbol{e}, \zeta) = \sum_{i\nu\sigma} \left(\epsilon_i^0 - \mu + \frac{1}{2}\tilde{U}_i \zeta_i \right) n_{i\nu\sigma} - \sum_{i\nu} \left(\frac{1}{2}\tilde{J}_i \xi_i \boldsymbol{e}_i + \boldsymbol{h}_i \right) \cdot \boldsymbol{m}_i + \sum_{i\nu j\nu'\sigma} t_{ij\sigma} a^{\dagger}_{i\nu\sigma} a_{j\nu'\sigma}. \tag{26}$$

Here $\boldsymbol{e}_i$ is the unit vector showing the direction of the rotated $\mathbf{z}$ axis on site i. It should be noted that the partition function $Z(\{\boldsymbol{e}_i\})$ does not have the rotational invariance since we neglected the transverse spin fluctuations on the rotated coordinates. The free energy F_{st}, which has the rotational invariance, is obtained by averaging $Z(\{\boldsymbol{e}_i\})$ over all the directions $\{\boldsymbol{e}_i\}$:

$$F_{\mathrm{st}} = -\beta^{-1} \ln \int \left[\prod_i^N \left(\frac{\beta \tilde{J}_i}{4\pi} \right)^{1/2} d\xi_i \, d\boldsymbol{e}_i \right] e^{-\beta E(\xi)}, \tag{27}$$

$$E(\boldsymbol{\xi}) = -\beta^{-1} \ln \mathrm{Tr}\{\exp[-\beta H_{\mathrm{st}}(\boldsymbol{\xi}, \zeta)]\} - \frac{1}{4} \sum_i (\tilde{U}_i \zeta_i^2 - \tilde{J}_i \xi_i^2). \tag{28}$$

Here $d\boldsymbol{e}_i = (4\pi)^{-1} \sin\theta_i \, d\theta_i \, d\phi_i$ and $\boldsymbol{\xi}_i = \xi_i \boldsymbol{e}_i$. We adopted the saddle-point approximation for the charge fields, so that $\zeta_i(\boldsymbol{\xi})$ is determined from the condition $\partial E / \partial \zeta_i = 0$:

$$\zeta_i(\boldsymbol{\xi}) = \langle n_i \rangle_0 = \frac{\mathrm{Tr}\{n_i \exp[-\beta H_{\mathrm{st}}(\boldsymbol{\xi}, \zeta)]\}}{\mathrm{Tr}\{\exp[-\beta H_{\mathrm{st}}(\boldsymbol{\xi}, \zeta)]\}}. \tag{29}$$

The local charge and local magnetic moment (LM) are obtained by taking the derivatives of F_{st} with respect to the atomic level ϵ_i^0 and the local magnetic field $\boldsymbol{h}_i$ as follows:

$$\langle n_i \rangle = \langle \zeta_i(\boldsymbol{\xi}) \rangle, \tag{30}$$

$$\langle \boldsymbol{m}_i \rangle = \left\langle \left(1 + \frac{4}{\beta \tilde{J}_i \xi_i^2} \right) \boldsymbol{\xi}_i \right\rangle. \tag{31}$$

Here the average $\langle \sim \rangle$ in the right-hand side of the above equations is defined by

$$\langle \sim \rangle = \frac{\int \left[\prod_j d\boldsymbol{\xi}_j \xi_j^{-2} \right] (\sim) e^{-\beta E(\boldsymbol{\xi})}}{\int \left[\prod_j d\boldsymbol{\xi}_j \xi_j^{-2} \right] e^{-\beta E(\boldsymbol{\xi})}}. \tag{32}$$

Note that we adopted the spherical coordinates in the above average $\langle \sim \rangle$. The local charge and spin fluctuations are obtained from the formulas $\langle n_i^2 \rangle = \langle n_i \rangle + 4 \partial F_{\mathrm{st}} / \partial U_i$ and $\langle \boldsymbol{m}_i^2 \rangle = 3\langle n_i \rangle - 4 \partial F_{\mathrm{st}} / \partial J_i$. The results are given by

$$\langle n_i^2 \rangle = \langle \zeta_i \rangle + \left(1 - \frac{1}{2D} \right) \langle \zeta_i^2 \rangle - \frac{1}{2D} \left(\langle \xi_i^2 \rangle - \frac{2}{\beta \tilde{J}_i} \right), \tag{33}$$

$$\langle \boldsymbol{m}_i^2 \rangle = 3\langle \zeta_i \rangle - \frac{3}{2D} \langle \zeta_i^2 \rangle + \left(1 + \frac{1}{2D} \right) \left(\langle \xi_i^2 \rangle - \frac{2}{\beta \tilde{J}_i} \right). \tag{34}$$

In order to simplify the actual calculations, we consider the limit $\tilde{U}_i \to \infty$, introducing charge potentials $\{w_i(\boldsymbol{\xi})\}$. These potentials are determined by the charge neutrality conditions.[46] Equation (28) is then written as follows:

$$E(\boldsymbol{\xi}) = \int d\omega \, f(\omega) \frac{D}{\pi} \mathrm{Im}\, \mathrm{Tr}[\ln(L^{-1} - t)] + \sum_i \left(-N_i w_i(\boldsymbol{\xi}) + \frac{1}{4} \tilde{J}_i \xi_i^2 \right). \tag{35}$$

Here $f(\omega)$ is the Fermi distribution function and $(t)_{i\nu\sigma j\nu'\sigma'} = t_{ij} \delta_{\nu\nu'} \delta_{\sigma\sigma'}$. N_i is the electron number on site i. The locator matrix L is defined by

$$(L^{-1})_{i\sigma j\sigma'} = [\omega + i\delta - \epsilon_i^0 + \mu - w_i(\boldsymbol{\xi})] \delta_{ij} \delta_{\sigma\sigma'} + \left(\frac{1}{2} \tilde{J}_i \boldsymbol{\xi}_i + \boldsymbol{h}_i \right) \cdot (\boldsymbol{\sigma})_{\sigma\sigma'} \delta_{ij}. \tag{36}$$

Here δ in $\omega + i\delta$ means an infinitesimal positive number.

B. Local moments in an effective medium

The pair distribution function of amorphous Fe, obtained from both the computer simulation[47] and the experiment,[48] shows that there exists a well-defined nearest-neighbor (NN) shell even in amorphous metals and alloys. We, therefore, take into account the local environment effects due to the NN atoms directly, and describe the effect of further distant atoms introducing two kinds of effective media.

We first introduce an inverse effective locator $\mathcal{L}_\sigma^{-1}$ into the first term in Eq. (35) to describe the diagonal disorder as an average medium and expand the deviation from $\mathcal{L}_\sigma^{-1}$ with respect to the sites. We can then rewrite the energy (35) in the form

$$E(\boldsymbol{\xi}) = \int d\omega \, f(\omega) \frac{D}{\pi} \mathrm{Im}\, \mathrm{Tr} \ln(\mathcal{L}^{-1} - t) F + \sum_i E_i(\boldsymbol{\xi}_i) + \Delta E(\boldsymbol{\xi}). \tag{37}$$

Here the coherent Green function F is defined by

$$F_{i\sigma j\sigma'}=[(\mathcal{L}^{-1}-t)]_{i\sigma i\sigma}\delta_{ij}\delta_{\sigma\sigma'}. \tag{38}$$

The first term in the right-hand-side of Eq. (37) is the zeroth-order term, which is described by the effective medium only. This term could be dropped from the expression of energy, since it does not play any role in the thermal average. The second term is the first-order correction consisting of the sum of the single-site energy $E_i(\boldsymbol{\xi}_i)$. It is given by

$$E_i(\boldsymbol{\xi}_i)=\int d\omega\ f(\omega)\frac{D}{\pi}\mathrm{Tr}^{(i)}\ln(L^{-1}-\mathcal{L}^{-1}+F^{-1}) - N_i w_i(\boldsymbol{\xi})+\frac{1}{4}\tilde{J}_i\xi_i^2. \tag{39}$$

The third term in the right-hand side of Eq. (37) is the higher-order correction. ΔE reduces to $\Sigma_{(i,j)}\Phi_{ij}(\boldsymbol{\xi}_i,\boldsymbol{\xi}_j)$ in the pair approximation, where all the higher-order terms are neglected by assuming small deviation from the effective medium. The pair energy functional $\Phi_{ij}(\boldsymbol{\xi}_i,\boldsymbol{\xi}_j)$ between sites i and j is given by

$$\Phi_{ij}(\boldsymbol{\xi}_i,\boldsymbol{\xi}_j)=\int d\omega\ f(\omega)\frac{D}{\pi}\mathrm{Im}\,\mathrm{Tr}^{(ij)}[\ln(1+\tilde{t}F')]. \tag{40}$$

Here $\mathrm{Tr}^{(ij)}$ denotes the trace over the subspace of sites i and j, and the off-diagonal coherent Green function is defined by

$$F'_{i\sigma j\sigma'}=[(\mathcal{L}^{-1}-t)]_{i\sigma j\sigma}(1-\delta_{ij})\delta_{\sigma\sigma'}, \tag{41}$$

and $\tilde{t}$ is the single-site t matrix defined by

$$\tilde{t}=[1+(L^{-1}-\mathcal{L}^{-1})F]^{-1}(L^{-1}-\mathcal{L}^{-1}). \tag{42}$$

Making use of Eq. (31), the thermal average of the central local moment is given as

$$\langle \boldsymbol{m}_0\rangle=\frac{\int d\boldsymbol{\xi}_0\xi_0^{-2}\left(1+\frac{4}{\beta\tilde{J}_0\xi_0^2}\right)\boldsymbol{\xi}_0 e^{-\beta E_0(\boldsymbol{\xi}_0)}\left\langle e^{-\beta\sum_{(i,j)}\Phi_{ij}(\boldsymbol{\xi}_i,\boldsymbol{\xi}_j)}\right\rangle_0'}{\int d\boldsymbol{\xi}_0\xi_0^{-2}e^{-\beta E_0(\boldsymbol{\xi}_0)}\left\langle e^{-\beta\sum_{(i,j)}\Phi_{ij}(\boldsymbol{\xi}_i,\boldsymbol{\xi}_j)}\right\rangle_0'}. \tag{43}$$

Here the average $\langle(\sim)\rangle_0'$ is defined by

$$\langle(\sim)\rangle_0'=\int\left[\prod_{i=1}^{N_s-1}p_i(\boldsymbol{\xi}_i)\,d\boldsymbol{\xi}_i\ \xi_i^{-2}\right](\sim), \tag{44}$$

and $p_i(\boldsymbol{\xi}_i)$ is the probability density for the single-site energy $E_i(\boldsymbol{\xi}_i)$

$$p_i(\boldsymbol{\xi}_i)=\frac{e^{-\beta E_i(\boldsymbol{\xi}_i)}}{\int d\boldsymbol{\xi}_i\xi_i^{-2}e^{-\beta E_i(\boldsymbol{\xi}_i)}}. \tag{45}$$

In the next step we treat the thermal average in Eq. (43). Since the direct integration of the type (44) is impossible, we make use of the following decoupling approximation for arbitrary function f, which is correct up to the second moment:

$$\langle f(\boldsymbol{\xi}_i)\rangle_0\equiv\int d\boldsymbol{\xi}_i\ p_i(\boldsymbol{\xi}_i)f(\boldsymbol{\xi}_i) =\sum_{\boldsymbol{s}_i}\frac{1}{8}\left(1+\frac{\langle\xi_{i\mathbf{z}}\rangle_0}{a_{i\mathbf{z}}}s_{i\mathbf{z}}\right)f(\{s_{i\alpha}a_{i\alpha}\}), \tag{46}$$

where $\Sigma_{\boldsymbol{s}_i}=\Sigma_{s_{i\mathbf{x}}=\pm1}\Sigma_{s_{i\mathbf{y}}=\pm1}\Sigma_{s_{i\mathbf{z}}=\pm1}$ and $a_{i\alpha}=\langle\xi_{i\alpha}^2\rangle_0^{1/2}$, $\langle\ \rangle_0$ denotes the thermal average with respect to the single-site energy on site i. Then we have

$$\langle \boldsymbol{m}_0\rangle=\frac{\int d\boldsymbol{\xi}_0\xi_0^{-2}\sum_{\{s_i\}}\left(1+\frac{4}{\beta\tilde{J}_0\xi_0^2}\right)\boldsymbol{\xi}_0\exp[-\beta\Psi(\boldsymbol{\xi}_0,\{s_{i\alpha}a_{i\alpha}\})]}{\int d\boldsymbol{\xi}_0\xi_0^{-2}\sum_{\{s_i\}}\exp[-\beta\Psi(\boldsymbol{\xi}_0,\{s_{i\alpha}a_{i\alpha}\})]}, \tag{47}$$

$$\Psi(\boldsymbol{\xi},\{s_{i\alpha}a_{i\alpha}\})=E_0(\boldsymbol{\xi})-\beta^{-1}\sum_i s_{i\mathbf{z}}\tanh^{-1}\frac{\langle\xi_{i\mathbf{z}}\rangle_0}{a_{i\mathbf{z}}}+\Delta E(\boldsymbol{\xi},\{s_{i\alpha}a_{i\alpha}\}), \tag{48}$$

where

$$\Delta E(\boldsymbol{\xi},\{s_{i\alpha}a_{i\alpha}\})=\sum_{i\neq 0}\Phi_{0i}^{(a)}(\boldsymbol{\xi})-\sum_{i\neq 0}\sum_{\alpha}^{\mathbf{x},\mathbf{y},\mathbf{z}}\left[\Phi_{0i\alpha}^{(e)}(\boldsymbol{\xi})+\sum_{j\neq 0,i}\mathcal{K}_{ij\alpha}\right]s_{i\alpha}$$
$$+\sum_{i\neq 0}\sum_{(\alpha,\gamma)}{}'\ \Phi_{0i\beta}^{(b)}(\boldsymbol{\xi})s_{i\alpha}s_{i\gamma}+\sum_{(i,j)}{}'\ \frac{1}{64}\sum_{\boldsymbol{\mu}_i\boldsymbol{\mu}_j}\Phi_{ij}(\{\mu_{i\alpha}a_{i\alpha}\},\{\mu_{j\alpha}a_{j\alpha}\})-\sum_{(i\alpha,j\gamma)}{}'\ \mathcal{J}_{ij\beta}s_{i\alpha}s_{j\gamma}$$
$$+\sum_{(i\alpha,j\beta,k\gamma)}{}'\ [\Phi_{0i}^{(c)}(\boldsymbol{\xi})+\mathcal{F}_{ki}^{(\alpha,\beta,\gamma)}\delta_{ij}+\mathcal{F}_{ij}^{(\beta,\gamma,\alpha)}\delta_{jk}+\mathcal{F}_{jk}^{(\gamma,\alpha,\beta)}\delta_{ki}]s_{i\alpha}s_{j\beta}s_{k\gamma}. \tag{49}$$

In Eq. (47), $\Sigma_{\{\boldsymbol{s}_i\}}$ denotes the sum over $\boldsymbol{s}_1$, $\boldsymbol{s}_2$, ... $\Sigma'_{(\alpha,\gamma)}$ in Eq. (49) means a summation over all the cyclic pairs of **x**, **y**, and **z**. $\Sigma'_{(i\alpha,j\gamma)}$ ($\Sigma'_{(i\alpha,j\beta,k\gamma)}$) denotes a summation with respect to all the pairs (triplets) of sites and components with $i\neq j$ and $\alpha\neq\gamma$ ($i\neq j\neq k$ and $\alpha\neq\beta\neq\gamma$), which are not related to site 0. The pair interactions $\Phi_{0j}^{(a)}(\boldsymbol{\xi})$, $\Phi_{0j\alpha}^{(e)}(\boldsymbol{\xi})$, $\Phi_{0j\beta}^{(b)}(\boldsymbol{\xi})$, $\Phi_{0j}^{(c)}(\boldsymbol{\xi})$, $\mathcal{K}_{ij\alpha}$, $\mathcal{J}_{ij\beta}$, and $\mathcal{F}_{ki}^{(\alpha,\beta,\gamma)}$ are defined, respectively, as follows:

$$\Phi_{0j}^{(a)}(\boldsymbol{\xi})=\frac{1}{8}\sum_{\boldsymbol{\mu}_j}\Phi_{0j}(\boldsymbol{\xi},\{\mu_{j\alpha}a_{j\alpha}\}), \tag{50}$$

$$\Phi_{0j\alpha}^{(e)}(\boldsymbol{\xi})=-\frac{1}{8}\sum_{\boldsymbol{\mu}_j}\mu_{j\alpha}\Phi_{0j}(\boldsymbol{\xi},\{\mu_{j\gamma}a_{j\gamma}\}), \tag{51}$$

$$\Phi_{0j\beta}^{(b)}(\boldsymbol{\xi})=\frac{1}{8}\sum_{\boldsymbol{\mu}_j}\mu_{j\alpha}\mu_{j\gamma}\Phi_{0j}(\boldsymbol{\xi},\{\mu_{j\delta}a_{j\delta}\}), \tag{52}$$

$$\Phi_{0j}^{(c)}(\boldsymbol{\xi})=\frac{1}{8}\sum_{\boldsymbol{\mu}_j}\mu_{j\mathbf{x}}\mu_{j\mathbf{y}}\mu_{j\mathbf{z}}\Phi_{0j}(\boldsymbol{\xi},\{\mu_{j\alpha}a_{j\alpha}\}), \tag{53}$$

$$\mathcal{K}_{ij\alpha}=\frac{1}{64}\sum_{\boldsymbol{\mu}_i}\sum_{\boldsymbol{\mu}_j}\mu_{i\alpha}\Phi_{ij}(\{\mu_{i\beta}a_{i\beta}\}\{\mu_{j\gamma}a_{j\gamma}\}), \tag{54}$$

$$\mathcal{J}_{ij\beta}=\frac{1}{64}\sum_{\boldsymbol{\mu}_i}\sum_{\boldsymbol{\mu}_j}\mu_{i\alpha}\mu_{j\gamma}\Phi_{ij}(\{\mu_{i\lambda}a_{i\lambda}\}\{\mu_{j\delta}a_{j\delta}\}), \tag{55}$$

$$\mathcal{F}_{ki}^{(\alpha,\beta,\gamma)}=\frac{1}{64}\sum_{\boldsymbol{\mu}_i}\sum_{\boldsymbol{\mu}_k}\mu_{i\alpha}\mu_{i\beta}\mu_{k\gamma}\Phi_{ik}(\{\mu_{i\delta}a_{i\delta}\}\{\mu_{k\nu}a_{k\nu}\}). \tag{56}$$

In the following, we make a molecular-field approximation for the thermal averages of LM's on the NN shell. The variables $s_{i\alpha}$, $s_{i\alpha}s_{j\gamma}$, and $s_{i\mathbf{x}}s_{j\mathbf{y}}s_{k\mathbf{z}}$ in Eq. (49) are replaced by their thermal averages:

$$\langle s_{i\alpha}\rangle=\frac{\langle m_{i\alpha}\rangle}{\tilde{a}_{i\alpha}}, \tag{57}$$

$$\langle s_{i\alpha}s_{j\gamma}\rangle=\frac{\langle m_{i\alpha}\rangle\langle m_{j\gamma}\rangle}{\tilde{a}_{i\alpha}\tilde{a}_{j\gamma}}, \tag{58}$$

$$\langle s_{i\mathbf{x}}s_{j\mathbf{y}}s_{k\mathbf{z}}\rangle=\frac{\langle m_{i\mathbf{x}}\rangle\langle m_{j\mathbf{y}}\rangle\langle m_{k\mathbf{z}}\rangle}{\tilde{a}_{i\mathbf{x}}\tilde{a}_{j\mathbf{y}}\tilde{a}_{k\mathbf{z}}}, \tag{59}$$

where

$$\tilde{a}_{j\alpha}=\left(1+\frac{4}{\beta\tilde{J}_j\langle\xi_j^2\rangle_0}\right)\langle\xi_{j\alpha}^2\rangle_0^{1/2}. \tag{60}$$

In Eqs. (58) and (59), we made use of the decoupling approximation $\langle s_{i\alpha}s_{j\gamma}\rangle\approx\langle s_{i\alpha}\rangle\langle s_{j\gamma}\rangle$ and $\langle s_{i\mathbf{x}}s_{j\mathbf{y}}s_{k\mathbf{z}}\rangle\approx\langle s_{i\mathbf{x}}\rangle\langle s_{j\mathbf{y}}\rangle\langle s_{k\mathbf{z}}\rangle$. Equations (47) and (48) reduce to

$$\langle\boldsymbol{m}_0\rangle=\frac{\int d\boldsymbol{\xi}\,\xi^{-2}\left(1+\frac{4}{\beta\tilde{J}\xi^2}\right)\boldsymbol{\xi}e^{-\beta\Psi(\boldsymbol{\xi})}}{\int d\boldsymbol{\xi}\,\xi^{-2}e^{-\beta\Psi(\boldsymbol{\xi})}}, \tag{61}$$

$$\Psi(\boldsymbol{\xi})=E_0(\boldsymbol{\xi})+\sum_{j=1}^{z}\left[\Phi_{0j}^{(a)}(\boldsymbol{\xi})-\sum_{\alpha}\Phi_{0j\alpha}^{(e)}(\boldsymbol{\xi})\frac{\langle m_{j\alpha}\rangle}{\tilde{a}_{j\alpha}}\right.$$
$$+\sum_{(\alpha,\gamma)}\Phi_{0j\delta}^{(b)}(\boldsymbol{\xi})\frac{\langle m_{j\alpha}\rangle\langle m_{j\gamma}\rangle}{\tilde{a}_{j\alpha}\tilde{a}_{j\gamma}}$$
$$\left.+\Phi_{0j}^{(c)}(\boldsymbol{\xi})\frac{\langle m_{j\mathbf{x}}\rangle\langle m_{j\mathbf{y}}\rangle\langle m_{j\mathbf{z}}\rangle}{\tilde{a}_{j\mathbf{x}}\tilde{a}_{j\mathbf{y}}\tilde{a}_{j\mathbf{z}}}\right]. \tag{62}$$

Here z is the number of atoms in the NN shell. $\Sigma_\alpha(\Sigma_{(\alpha\gamma)})$ denotes the sum over the **x**, **y**, and **z** components [(**yz**), (**zx**), and (**xy**) pairs]. We took into account the pair interactions in the NN shell and neglected the direct interactions with the atoms outside the shell because of the damping effect in the disordered systems.

The final expression of the single-site energy $E_0(\boldsymbol{\xi})$ in Eq. (62) is given by

$$E_0(\boldsymbol{\xi})=\int d\omega\ f(\omega)\frac{D}{\pi}\mathrm{Im}\ln\left[(\delta L_{0\uparrow}^{-1}+F_{00\uparrow}^{-1})(\delta L_{0\downarrow}^{-1}+F_{00\downarrow}^{-1})\right.$$
$$\left.-\frac{1}{4}\tilde{J}_0^2\xi_\perp^2\right]-N_0w_0(\boldsymbol{\xi})+\frac{1}{4}\tilde{J}_0\xi^2, \tag{63}$$

where

$$\delta L_{j\sigma}^{-1}=(L^{-1})_{j\sigma j\sigma}-\mathcal{L}_\sigma^{-1}, \tag{64}$$

$$F_{jj\sigma}\equiv F_{j\sigma j\sigma}=[(\mathcal{L}^{-1}-t)^{-1}]_{j\sigma j\sigma}, \tag{65}$$

and

$$\xi_\perp^2=\xi_{\mathbf{x}}^2+\xi_{\mathbf{y}}^2. \tag{66}$$

The pair energies $\Phi_{0j}^{(a)}(\boldsymbol{\xi})$, $\Phi_{0j\alpha}^{(e)}(\boldsymbol{\xi})$, $\Phi_{0j\delta}^{(b)}(\boldsymbol{\xi})$, and $\Phi_{0j}^{(c)}(\boldsymbol{\xi})$ are calculated via Eqs. (50)–(53) from $\Phi_{0j}(\boldsymbol{\xi},\boldsymbol{\xi}_j)$, which is given by

$$\begin{aligned}\Phi_{0j}(\boldsymbol{\xi},\boldsymbol{\xi}_j) &= \int d\omega\, f(\omega)\frac{D}{\pi}\mathrm{Im}\ln\Bigg[1-\sum_{\sigma}(\tilde{t}_0)_{\sigma\sigma}F_{0j\sigma}F_{j0\sigma}(\tilde{t}_j)_{\sigma\sigma} \\ &\quad -F_{0j\uparrow}F_{j0\downarrow}\frac{\tilde{J}_0\tilde{J}_j}{2\tilde{R}_0 2\tilde{R}_j}(\xi_+\xi_{j-}+\xi_-\xi_{j+})+(F_{0j\uparrow}F_{j0\downarrow})^2 \\ &\quad \times\left\{(\tilde{t}_0)_{\uparrow\uparrow}(\tilde{t}_0)_{\downarrow\downarrow}-\frac{\tilde{J}_0^2\xi_{\perp}^2}{4\tilde{R}_0^2}\right\}\left\{(\tilde{t}_j)_{\uparrow\uparrow}(\tilde{t}_j)_{\downarrow\downarrow}-\frac{\tilde{J}_j^2\xi_{j\perp}^2}{4\tilde{R}_j^2}\right\}\Bigg].\end{aligned} \tag{67}$$

Here we omitted the primes in $F_{0j\sigma}{}'=F_{j0\sigma}{}'$ for brevity. $\xi_{j\pm}=\xi_{j\mathbf{x}}\pm i\xi_{j\mathbf{y}}$, $(\tilde{t}_j)_{\sigma\sigma'}$ is the single-site t matrix whose diagonal component is given by

$$(\tilde{t}_j)_{\sigma\sigma}=\frac{\delta L_{j\sigma}^{-1}+\left(\delta L_{j\uparrow}^{-1}\delta L_{j\downarrow}^{-1}-\frac{1}{4}\tilde{J}_j^2\xi_{j\perp}^2\right)F_{jj\sigma}}{\tilde{R}_j}, \tag{68}$$

$$\tilde{R}_j=(1+\delta L_{j\uparrow}^{-1}F_{jj\uparrow})(1+\delta L_{j\downarrow}^{-1}F_{jj\downarrow})-\frac{1}{4}\tilde{J}_j^2\xi_{j\perp}^2F_{jj\uparrow}F_{jj\downarrow}. \tag{69}$$

The effective medium $\mathcal{L}_{\sigma}^{-1}$ is determined so that the averaged single-site t matrix vanishes:

$$[\langle(\tilde{t}_0)_{\sigma\sigma}(\boldsymbol{\xi})\rangle]_{\mathrm{s}}=0. \tag{70}$$

Here $\langle\cdots\rangle$ means the thermal average with respect to $\Psi(\boldsymbol{\xi})$. $[\,]_{\mathrm{s}}$ denotes the structural average. Equation (70) is called the coherent potential approximation (CPA) equation.[49]

The central LM (61) depends on the structural disorder outside the NN shell via the coherent Green functions $F_{00\sigma}$, $F_{0j\sigma}(=F_{j0\sigma})$, and $F_{jj\sigma}$ in Eq. (62). These Green functions are treated by the Bethe approximation.[50] Making use of the locator expansion, we have the relations

$$F_{00}=\mathcal{L}+\mathcal{L}\sum_{j\neq 0}t_{0j}F_{j0}, \tag{71}$$

$$F_{j0}=\mathcal{L}t_{j0}F_{00}+\mathcal{L}\mathcal{S}_jF_{j0}+\mathcal{L}\sum_{i\neq j,0}\mathcal{T}_{ji}F_{i0}. \tag{72}$$

Here we have omitted the spin suffix σ for brevity and neglected the transfer integrals between the central atoms and the atoms outside the NN shell. The self-energy $\mathcal{S}_j(\mathcal{T}_{ji})$ consists of the sum of all the paths that start from site j and end at site $j(i)$ without returning to the cluster on the way. Note that all the information outside the cluster is contained in $\mathcal{S}_j$ and $\mathcal{T}_{ji}$.

When we take the structural average outside the cluster, we neglect the last term on the right-hand side of Eq. (72), and replace $\mathcal{S}_j$ with $\mathcal{S}$, an effective medium for the structural disorder. We then obtain

$$F_{00\sigma}=\left(\mathcal{L}_{\sigma}^{-1}+\sum_{j=1}^{z}\frac{t_{j0}^2}{\mathcal{L}_{\sigma}^{-1}-\mathcal{S}_{\sigma}}\right)^{-1}, \tag{73}$$

$$F_{j0\sigma}=\frac{t_{j0}}{\mathcal{L}_{\sigma}^{-1}-\mathcal{S}_{\sigma}}F_{00\sigma}. \tag{74}$$

The diagonal Green functions $F_{jj\sigma}$ in the NN shell, on the other hand, are approximated by the averaged one

$$F_{\sigma}=[F_{jj\sigma}]_{\mathrm{s}}=\int\frac{[\rho(\epsilon)]_{\mathrm{s}}d\epsilon}{\mathcal{L}_{\sigma}^{-1}-\epsilon}. \tag{75}$$

Here $\rho(\epsilon)$ denotes the noninteracting density-of-states (DOS) for the amorphous system. The effective medium $\mathcal{S}_{\sigma}$ is determined from the condition that the structural average of the central Green function $F_{00\sigma}$, should be identical with the neighboring one

$$[F_{00\sigma}]_{\mathrm{s}}=\int\frac{[\rho(\epsilon)]_{\mathrm{s}}\,d\epsilon}{\mathcal{L}_{\sigma}^{-1}-\epsilon}. \tag{76}$$

C. Distribution function method

The central LM in Eq. (61) is now determined by the coordination number z on the NN shell, the neighboring LM's $\{\langle\boldsymbol{m}_j\rangle\}$, the square of transfer integrals $\{y_j=t_{j0}^2\}$, the effective medium $\mathcal{L}_{\sigma}^{-1}$ due to the spin fluctuations, and the effective medium $\mathcal{S}_{\sigma}$ due to the structural disorder outside the NN shell:

$$\langle\boldsymbol{m}_0\rangle=\langle\boldsymbol{m}_0\rangle(z,\{\langle\boldsymbol{m}_j\rangle\},\{y_j\},\{\mathcal{S}_{\sigma}\},\{\mathcal{L}_{\sigma}^{-1}\}). \tag{77}$$

The structural disorder causes the distribution $g(\langle\boldsymbol{m}_j\rangle)$ of the LM at the neighboring site j, the distribution $p_{\mathrm{s}}(y_j)$ for the square of the transfer integral, and the distribution of the coordination number $p(z)$. Since the distribution for the central LM should be identical with those for the surrounding LM's, we obtain the following integral equation for the LM distribution:

$$\begin{aligned}g(\boldsymbol{M}) &= \sum_z p(z)\int\delta(\boldsymbol{M}-\langle\boldsymbol{m}_0\rangle) \\ &\quad\times\prod_{j=1}^{z}[p_{\mathrm{s}}(y_j)\,dy_j\;g(\boldsymbol{m}_j)\,d\boldsymbol{m}_j].\end{aligned} \tag{78}$$

The effective media $\mathcal{L}_{\sigma}^{-1}$ and $\mathcal{S}_{\sigma}$ are self-consistently determined from Eqs. (70) and (76):

$$\int\langle(\tilde{t}_0)_{\sigma\sigma}\rangle\prod_{j=1}^{z}[p_{\mathrm{s}}(y_j)\,dy_j\,g(\boldsymbol{m}_j)\,d\boldsymbol{m}_j]=0, \tag{79}$$

$$\int F_{00\sigma}\prod_{j=1}^{z}[p_{\mathrm{s}}(y_j)dy_j]=\int\frac{[\rho(\epsilon)]_{\mathrm{s}}d\epsilon}{\mathcal{L}_{\sigma}^{-1}-\epsilon}. \tag{80}$$

The LM distribution $g(\boldsymbol{M})$ and the effective media $\mathcal{L}_\sigma^{-1}$ and $\mathcal{S}_\sigma$, are determined by solving Eqs. (78), (79), and (80). The average magnetization $[\langle m_{\mathbf{z}}\rangle]_{\mathrm{s}}$, and the SG order parameters for each direction $[\langle m_\alpha\rangle^2]_{\mathrm{s}}^{1/2}$ $(\alpha=\mathbf{x},\mathbf{y},\mathbf{z})$, are obtained from the distribution $g(\boldsymbol{M})$ as follows:

$$[\langle m_{\mathbf{z}}\rangle]_{\mathrm{s}}=\int M_{\mathbf{z}}g(\boldsymbol{M})\,d\boldsymbol{M}, \tag{81}$$

$$[\langle m_\alpha\rangle^2]_{\mathrm{s}}^{1/2}=\int M_\alpha^2 g(\boldsymbol{M})\,d\boldsymbol{M}. \tag{82}$$

Since Eqs. (78), (79), and (80) include $4z$-fold integrals, it is difficult to solve the equations without making further approximations. We adopt the following decoupling approximation in Eqs. (78)–(82), which is correct up to the second moment

$$\begin{aligned}\int f(\boldsymbol{m})g(\boldsymbol{m})d\boldsymbol{m}&\approx\sum_{\boldsymbol{\nu}}\frac{1}{8}\left(1+\nu_{\mathbf{z}}\frac{[\langle m_{\mathbf{z}}\rangle]_{\mathrm{s}}}{[\langle m_{\mathbf{z}}\rangle^2]_{\mathrm{s}}^{1/2}}\right)\\&\quad\times f(\nu_{\mathbf{x}}[\langle m_{\mathbf{x}}\rangle^2]_{\mathrm{s}}^{1/2},\nu_{\mathbf{y}}[\langle m_{\mathbf{y}}\rangle^2]_{\mathrm{s}}^{1/2},\nu_{\mathbf{z}}[\langle m_{\mathbf{z}}\rangle^2]_{\mathrm{s}}^{1/2}),\end{aligned} \tag{83}$$

$$\int (y-[y]_{\mathrm{s}})^{2n+k}p_{\mathrm{s}}(y)\,dy\approx[(\delta y)^2]_{\mathrm{s}}^n 0^k. \tag{84}$$

Here we assumed that the spontaneous magnetization appears along the $\mathbf{z}$ axis and the distribution $g(\boldsymbol{m})$ shows an uniaxial symmetry around the $\mathbf{z}$ axis. $\Sigma_{\boldsymbol{\nu}}=\Sigma_{\nu_{\mathbf{x}}=\pm1}\Sigma_{\nu_{\mathbf{y}}=\pm1}\Sigma_{\nu_{\mathbf{z}}=\pm1}$ and $k=0$ or 1. $[y]_{\mathrm{s}}$ is a mean square of a transfer integral, and $[(\delta y)^2]_{\mathrm{s}}$ is the fluctuation around $[y]_{\mathrm{s}}$, which is calculated from the fluctuations of the interatomic distance R as follows:

$$\frac{[(\delta y)^2]_{\mathrm{s}}^{1/2}}{[y]_{\mathrm{s}}}=2\kappa\,\frac{[(\delta R)^2]_{\mathrm{s}}^{1/2}}{[R]_{\mathrm{s}}}. \tag{85}$$

Here we adopted Heine's law $t(R)\equiv t_{j0}\propto R^{-\kappa}$ $(\kappa=3.8)$.[51,52] $[R]_{\mathrm{s}}$ and $[(\delta R)^2]_{\mathrm{s}}^{1/2}$ denote the average interatomic distance and its fluctuation.

Substituting Eq. (78) after the decoupling approximation into Eqs. (81) and (82), we obtain the self-consistent equations for $[\langle m_\alpha\rangle^n]_{\mathrm{s}}$ as follows:

$$\begin{aligned}[\langle m_\alpha\rangle^n]_{\mathrm{s}}&=\int M_\alpha^n g(\boldsymbol{M})\,d\boldsymbol{M}\\&=\sum_z p(z)\sum_{i=0}^{z}\Gamma\left(i,z,\frac{1}{2}\right)\sum_{k_{\mathbf{z}}}^{i}\sum_{l_{\mathbf{z}}}^{z-i}\Gamma(k_{\mathbf{z}},i,q_{\mathbf{z}})\Gamma(l_{\mathbf{z}},z-i,q_{\mathbf{z}})\sum_{\{k_{\mathbf{x}},k_{\mathbf{y}}\}}\Gamma\left(k_{\mathbf{x}},k_{\mathbf{z}},\frac{1}{2}\right)\Gamma\left(k_{\mathbf{y}},k_{\mathbf{x}},\frac{1}{2}\right)\Gamma\left(k'_{\mathbf{y}},k_{\mathbf{z}}-k_{\mathbf{x}},\frac{1}{2}\right)\\&\quad\times\Gamma\left(k'_{\mathbf{x}},i-k_{\mathbf{z}},\frac{1}{2}\right)\Gamma\left(k''_{\mathbf{y}},k'_{\mathbf{x}},\frac{1}{2}\right)\Gamma\left(k'''_{\mathbf{y}},i-k_{\mathbf{z}}-k'_{\mathbf{x}},\frac{1}{2}\right)\sum_{\{l_{\mathbf{x}},l_{\mathbf{y}}\}}\Gamma\left(l_{\mathbf{x}},l_{\mathbf{z}},\frac{1}{2}\right)\Gamma\left(l_{\mathbf{y}},l_{\mathbf{x}},\frac{1}{2}\right)\Gamma\left(l'_{\mathbf{y}},l_{\mathbf{z}}-l_{\mathbf{x}},\frac{1}{2}\right)\\&\quad\times\Gamma\left(l'_{\mathbf{x}},z-i-l_{\mathbf{z}},\frac{1}{2}\right)\Gamma\left(l''_{\mathbf{y}},l'_{\mathbf{x}},\frac{1}{2}\right)\Gamma\left(l'''_{\mathbf{y}},z-i-l_{\mathbf{z}}-l'_{\mathbf{x}},\frac{1}{2}\right)\langle m_\alpha\rangle(z,i,\{k\},\{l\})^n,\end{aligned} \tag{86}$$

$$\langle m_\alpha\rangle(z,i,\{k\},\{l\})=\frac{\displaystyle\int d\boldsymbol{\xi}\,\xi^{-2}\left(1+\frac{4}{\beta\tilde{J}\xi^2}\right)\boldsymbol{\xi}\exp[-\beta\Psi(\boldsymbol{\xi},z,i,\{k\},\{l\})]}{\displaystyle\int d\boldsymbol{\xi}\,\xi^{-2}\exp[-\beta\Psi(\boldsymbol{\xi},z,i,\{k\},\{l\})]}, \tag{87}$$

$$\begin{aligned}\Psi(\boldsymbol{\xi},z,i,\{k\},\{l\})&=E_0(\boldsymbol{\xi},z,i)+i\Phi_+^{(a)}(\boldsymbol{\xi},z,i)+(z-i)\Phi_-^{(a)}(\boldsymbol{\xi},z,i)-[(2k_{\mathbf{z}}-i)\Phi_{\mathbf{z}+}^{(e)}(\boldsymbol{\xi},z,i)+(2l_{\mathbf{z}}-z+i)\Phi_{\mathbf{z}-}^{(e)}(\boldsymbol{\xi},z,i)]v_{\mathbf{z}}\\&\quad-[\{2(k_{\mathbf{x}}+k'_{\mathbf{x}})-i\}\Phi_{\mathbf{x}+}^{(e)}(\boldsymbol{\xi},z,i)+\{2(l_{\mathbf{x}}+l'_{\mathbf{x}})-z+i\}\Phi_{\mathbf{x}-}^{(e)}(\boldsymbol{\xi},z,i)]v_{\mathbf{x}}-[\{2(k_{\mathbf{y}}+k'_{\mathbf{y}}+k''_{\mathbf{y}}+k'''_{\mathbf{y}})-i\}\Phi_{\mathbf{y}+}^{(e)}(\boldsymbol{\xi},z,i)\\&\quad+\{2(l_{\mathbf{y}}+l'_{\mathbf{y}}+l''_{\mathbf{y}}+l'''_{\mathbf{y}})-z+i\}\Phi_{\mathbf{y}-}^{(e)}(\boldsymbol{\xi},z,i)]v_{\mathbf{y}}+[\{2(k_{\mathbf{x}}-k_{\mathbf{z}}-k'_{\mathbf{x}})+i\}\Phi_{\mathbf{y}+}^{(b)}(\boldsymbol{\xi},z,i)\\&\quad+\{2(l_{\mathbf{x}}-l_{\mathbf{z}}-l'_{\mathbf{x}})+z-i\}\Phi_{\mathbf{y}-}^{(b)}(\boldsymbol{\xi},z,i)]v_{\mathbf{z}}v_{\mathbf{x}}+[\{2(k_{\mathbf{y}}-k_{\mathbf{x}}-k'_{\mathbf{y}}+k''_{\mathbf{y}}-k'_{\mathbf{x}}-k'''_{\mathbf{y}})+i\}\Phi_{\mathbf{z}+}^{(b)}(\boldsymbol{\xi},z,i)\\&\quad+\{2(l_{\mathbf{y}}-l_{\mathbf{x}}-l'_{\mathbf{y}}+l''_{\mathbf{y}}-l'_{\mathbf{x}}-l'''_{\mathbf{y}})+z-i\}\Phi_{\mathbf{z}-}^{(b)}(\boldsymbol{\xi},z,i)]v_{\mathbf{x}}v_{\mathbf{y}}+[\{2(k_{\mathbf{y}}+k'_{\mathbf{y}}-k_{\mathbf{z}}-k''_{\mathbf{y}}-k'''_{\mathbf{y}})+i\}\Phi_{\mathbf{x}+}^{(b)}(\boldsymbol{\xi},z,i)\\&\quad+\{2(l_{\mathbf{y}}+l'_{\mathbf{y}}-l_{\mathbf{z}}-l''_{\mathbf{y}}-l'''_{\mathbf{y}})+z-i\}\Phi_{\mathbf{x}-}^{(b)}(\boldsymbol{\xi},z,i)]v_{\mathbf{y}}v_{\mathbf{z}}+[\{2(k_{\mathbf{y}}-k_{\mathbf{x}}-k'_{\mathbf{y}}+k_{\mathbf{z}}-k''_{\mathbf{y}}+k'_{\mathbf{x}}+k'''_{\mathbf{y}})-i\}\Phi_+^{(c)}(\boldsymbol{\xi},z,i)\\&\quad+\{2(l_{\mathbf{y}}-l_{\mathbf{x}}-l'_{\mathbf{y}}+l_{\mathbf{z}}-l''_{\mathbf{y}}+l'_{\mathbf{x}}+l'''_{\mathbf{y}})-z+i\}\Phi_-^{(c)}(\boldsymbol{\xi},z,i)]v_{\mathbf{x}}v_{\mathbf{y}}v_{\mathbf{z}},\end{aligned} \tag{88}$$

$$q_z=\frac{1}{2}\left(1+\frac{[\langle m_{\mathbf{z}}\rangle]_{\mathrm{s}}}{[\langle m_{\mathbf{z}}\rangle^2]_{\mathrm{s}}^{1/2}}\right), \tag{89}$$

$$v_\alpha = \frac{[\langle m_\alpha \rangle^2]_s^{1/2}}{\tilde{a}_\alpha}. \tag{90}$$

Here we adopted the distribution $p(z)=([z^*]+1-z^*)\delta_{z,[z^*]}+(z^*-[z^*])\delta_{z,[z^*]+1}$ in the actual calculations. z^* denotes the average coordination number, and [ ] denotes Gauss's notation. $\Gamma(i,z,p)$, in Eq. (86), is the binomial distribution function defined by $[z!/i!(z-i)!]p^i(1-p)^{z-i}$. $\Sigma_{\{k_x,k_y\}}$ and $\Sigma_{\{l_x,l_y\}}$ are defined as follows:

$$\sum_{\{k_x,k_y\}} = \sum_{k_x=0}^{k_z} \sum_{k_y=0}^{k_x} \sum_{k_y'=0}^{k_z-k_x} \sum_{k_x'=0}^{i-k_z} \sum_{k_y''=0}^{k_x'} \sum_{k_y'''=0}^{i-k_z-k_x'}, \tag{91}$$

$$\sum_{\{l_x,l_y\}} = \sum_{l_x=0}^{l_z} \sum_{l_y=0}^{l_x} \sum_{l_y'=0}^{l_z-l_x} \sum_{l_x'=0}^{z-i-l_z} \sum_{l_y''=0}^{l_x'} \sum_{l_y'''=0}^{z-i-l_z-l_x'}. \tag{92}$$

In the present approximation, the local environments inside the NN shell are described via the NN transfer integrals by the contraction $(-[(\delta R)^2]_s^{1/2})$ of the NN interatomic distance R from the average value $[R]_s$ and the stretch $([(\delta R)^2]_s^{1/2})$ of the distance R. Thus, the local structure is specified by means of the number of contracted pairs (i) between the central atom and the atoms on the NN shell. Since the local structure is realized with the probability $\Gamma(i,z,1/2)$, the LM's are averaged with respect to the binomial distribution in Eq. (86). The single-site energy and pair energies are then characterized by i, so that the notations $E_0(\boldsymbol{\xi},z,i)$, $\Phi_\pm^{(a)}(\boldsymbol{\xi},z,i)$, $\Phi_{\alpha\pm}^{(e)}(\boldsymbol{\xi},z,i)$, $\Phi_{\alpha\pm}^{(b)}(\boldsymbol{\xi},z,i)$, and $\Phi_\pm^{(c)}(\boldsymbol{\xi},z,i)$ are used in Eq. (88). Here the subscript $+(-)$ denotes the contracted (stretched) pair.

The parameter q_z, defined by Eq. (89), is interpreted as the probability that the $\mathbf{z}$ component of the fictitious spin $[\langle m_z \rangle^2]_s^{1/2}$ points up on a site of the NN shell. The probability of finding k_z up spins among i contracted atoms on the NN shell is then given by $\Gamma(k_z,i,q_z)$ and the probability of finding l_z up spins among $z-i$ stretched atoms is given by $\Gamma(l_z,z-i,q_z)$. Therefore, the LM's are averaged over these binomial distributions in Eq. (86). In the similar manner, the probabilities of finding positive transverse spin components are given by the other binomial distributions in Eq. (86).

The average central local moment $[\langle m_z \rangle]_s$ is obtained by averaging $\langle m_z \rangle(z,i,\{k\},\{l\})$ over the 10^7 configurations of the local atomic and spin degrees of freedom on the NN shell. We, therefore, make use of Monte Carlo sampling for the polynomial distribution in Eq. (86) in the numerical calculations of the central LM. Note that the central LM is written by the polynomial distribution as follows:

$$[\langle m_\alpha \rangle^n]_s = \int M_\alpha^n g(\boldsymbol{M})\, d\boldsymbol{M}$$
$$= \sum_z p(z) \sum_{z=\Sigma_\nu k_\nu} \frac{z!}{\left[\prod_{\nu=1}^{16} k_\nu!\right]} \times \left[\prod_{\nu=1}^{16} q_\nu^{k_\nu}\right] \langle m_\alpha \rangle(z,\{k_\nu\})^n. \tag{93}$$

Here $\Sigma_{z=\Sigma_\nu k_\nu}$ denotes the summation with respect to the integer variables $\{k_\nu\}$ ($\nu=1\sim16$) which run over the range $\{0\leqslant k_\nu \leqslant z\}$ under the constraint $z=\Sigma_{\nu=1}^{16} k_\nu$. The probabilities $\{q_\nu\}(\nu=1\sim16)$ are given by the formulas $q_\nu=(\frac{1}{2})^3 q_z(\nu=1\sim8)$ and $q_\nu=(\frac{1}{2})^3(1-q_z)(\nu=9\sim16)$, respectively.

By making use of the same decoupling approximations used as the above, we obtain a simplified CPA equation from Eq. (79):

$$\sum_{\nu=\pm1} \frac{1}{2}\left(1+\nu\frac{[\langle \xi_z \rangle]_s}{[\langle \xi_z^2 \rangle]_s^{1/2}}\right)(G)_{\sigma\sigma}([\langle \xi^2 \rangle]_s, \nu[\langle \xi_z^2 \rangle]_s^{1/2}) = F_\sigma, \tag{94}$$

where

$$(G)_{\sigma\sigma}([\langle \xi^2 \rangle]_s, \nu[\langle \xi_z^2 \rangle]_s^{1/2}) = F_\sigma \frac{1+\delta L_{-\sigma}^{-1}([\langle \xi^2 \rangle]_s, \nu[\langle \xi_z^2 \rangle]_s^{1/2})F_{-\sigma}}{\tilde{R}_0([\langle \xi^2 \rangle]_s, \nu[\langle \xi_z^2 \rangle]_s^{1/2})}. \tag{95}$$

In the same way, Eq. (80) for the self-energy reduces to the following equation:

$$\sum_{\nu=\pm1} \frac{1}{2}\left\{\mathcal{L}_\sigma^{-1} - [\theta]_s\left(1+\nu\frac{[(\delta\theta)^2]_s^{1/2}}{[\theta]_s}\right)(\mathcal{L}_\sigma^{-1}-\mathcal{S}_\sigma)^{-1}\right\}^{-1} = F_\sigma. \tag{96}$$

Here θ and $\delta\theta$ are defined by $\theta=\Sigma_j t_{j0}^2=\Sigma_j y_j$ and $\delta\theta=\theta-[\theta]_s$, respectively. The expression for $[(\delta\theta)^2]_s^{1/2}/[\theta]_s$ is given by

$$\frac{[(\delta\theta)^2]_s}{[\theta]_s^2} = \frac{[(\delta y)^2]_s}{z^*[y]_s^2} + \frac{[(\delta z)^2]_s}{z^{*2}}, \tag{97}$$

where $\delta z=z-z^*$, and $[(\delta y)^2]_s/[y]_s^2$ is obtained from $[(\delta R)^2]_s^{1/2}/[R]_s$ via Eq. (85).

The magnetization $[\langle m_z \rangle]_s$, the SG order parameters $[\langle m_z \rangle^2]_s^{1/2}$ and $[\langle m_x \rangle^2]_s^{1/2}$ $(=[\langle m_y \rangle^2]_s^{1/2})$, and the effective media $\mathcal{L}_\sigma^{-1}$ and $\mathcal{S}_\sigma$ are determined by solving Eqs. (93), (94), and (96) self-consistently. The self-consistent equations take into account the fluctuations of local moments due to the structural disorder and thus can describe the itinerant electron SG in amorphous transition metals. Since the transverse components of local moments are taken into account in the present theory, the self-consistent equations have solutions; the noncollinear SG $\{[\langle m_z \rangle]_s=0,\ [\langle m_\alpha \rangle^2]_s^{1/2}\neq0(\alpha=\mathbf{x},\mathbf{y},\mathbf{z})\}$, the noncollinear ferromagnetism $\{[\langle m_z \rangle]_s\neq0,\ [\langle m_\alpha \rangle^2]_s^{1/2}\neq0(\alpha=\mathbf{x},\mathbf{y},\mathbf{z})\}$, in addition to the collinear SG $\{[\langle m_z \rangle]_s=0,\ [\langle m_z \rangle^2]_s^{1/2}\neq0,\ [\langle m_\alpha \rangle^2]_s^{1/2}=0(\alpha=\mathbf{x},\mathbf{y})\}$, the collinear ferromagnetism $\{[\langle m_z \rangle]_s\neq0,\ [\langle m_z \rangle^2]_s^{1/2}\neq0,\ [\langle m_\alpha \rangle^2]_s^{1/2}=0(\alpha=\mathbf{x},\mathbf{y})\}$, and the paramagnetism $\{[\langle m_z \rangle]_s=0,\ [\langle m_\alpha \rangle^2]_s^{1/2}=0(\alpha=\mathbf{x},\mathbf{y},\mathbf{z})\}$.

In the actual calculations of the self-consistent equations, the input parameters describing the amorphous structure and the electronic states are necessary. The former includes the average coordination number z^* and the fluctuation of the

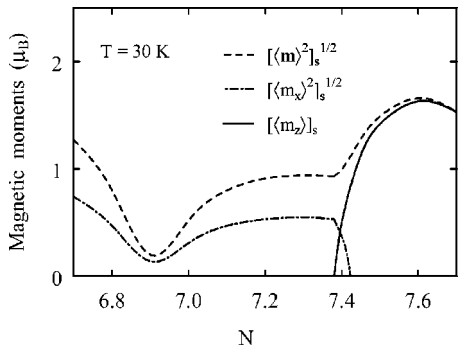

FIG. 1. Total spin-glass order parameter $[\langle \mathbf{m} \rangle^2]_s^{1/2}$, the transverse spin-glass order parameter $[\langle m_x \rangle^2]_s^{1/2}$, and the magnetization $[\langle m_z \rangle]_s$ as functions of *d* electron number *N* at 30 K.

interatomic distance $[(\delta R)^2]_s^{1/2}/[R]_s$; the latter includes the *d* electron number *N*, the effective exchange energy parameter $\tilde{J}$, and the noninteracting DOS $[\rho(\epsilon)]_s$.

III. NUMERICAL RESULTS

We have performed the numerical calculations varying the *d* electron number, temperature, and volume in the vicinity of the *d* electron number of pure amorphous Fe. We adopted the DOS for amorphous Fe, which was calculated by Fujiwara[53] with the use of the relaxed dense random packing of hard spheres (DRPHS) model, consisting of 1500 atoms and the tight-binding LMTO recursion method for electronic structure calculations. The structural averages over 10^7 local atomic and spin configurations in Eq. (93) were calculated by means of a 32 000 Monte Carlo sampling. The calculations with the use of a 480 000 Monte Carlo sampling were also performed at some representative points to test the numerical accuracy. We have confirmed that the absolute error of the former is less than $0.01\mu_B$ when compared to the latter.

A. d electron number and temperature dependencies

We examined the magnetic properties of amorphous transition metals as a function of the *d* electron number *N* and temperature *T*. In the calculations, we adopted the average coordination number $z^*=11.5$, estimated from the viewpoint of the DRPHS model.[19] The effective exchange energy parameter $\tilde{J}=0.059$ Ry was chosen so as to reproduce the observed ground-state magnetization $2.216\mu_B$ for the bcc Fe,[13] and the fluctuation of interatomic distances $[(\delta R)^2]_s^{1/2}/[R]_s = 0.067$ was estimated from the first peak in the theoretical[47] and experimental[48] pair distribution functions, all of which were used in our previous calculations.[23]

Figure 1 shows the calculated magnetization $[\langle m_z \rangle]_s$, the spin-glass (SG) order parameter $[\langle \boldsymbol{m} \rangle^2]_s^{1/2}$, and its transverse component $[\langle m_x \rangle^2]_s^{1/2}$ $(=[\langle m_y \rangle^2]_s^{1/2})$ as functions of *d* electron number *N* at 30 K.

The calculated magnetization $[\langle m_z \rangle]_s$ shows a maximum at a *d* electron number around $N=7.6$ and rapidly decreases with decreasing the *d* electron number towards amorphous Fe ($N \sim 7.0$). The magnetization curve is qualitatively the same as that obtained by the collinear calculations and is well understood by the main peak position of the noninteracting DOS for amorphous transition metals.[14]

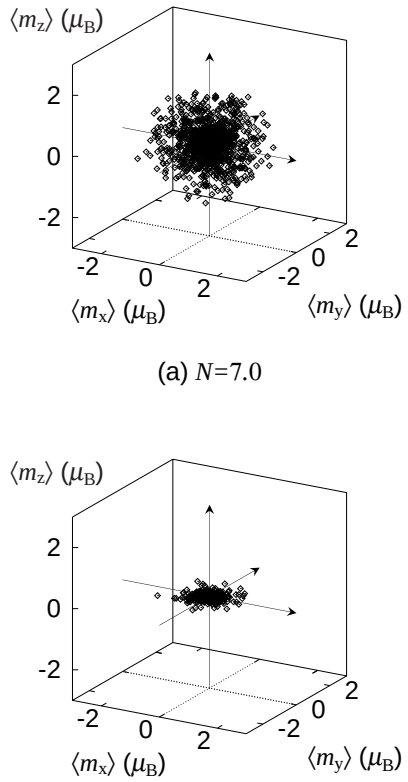

FIG. 2. Distribution of local moments at 30 K for *d* electron numbers (a) $N=7.0$ and (b) $N=6.9$. Here 4000 data points among 32 000 Monte Carlo samplings are shown.

In the region $N \geqslant 7.43$, the collinear ferromagnetism is realized, as indicated by the zero value of the transverse SG order parameter $[\langle m_x \rangle^2]_s^{1/2}$ $(=[\langle m_y \rangle^2]_s^{1/2})$. The ferromagnetism becomes noncollinear in the region $7.38 \leqslant N \leqslant 7.43$, where the transverse SG order parameter $[\langle m_x \rangle^2]_s^{1/2}$ becomes finite in the presence of the magnetization $[\langle m_z \rangle]_s$. At $N=7.38$, the magnetization disappears while both the total and transverse SG order parameters ($[\langle \boldsymbol{m} \rangle^2]_s^{1/2}$ and $[\langle m_x \rangle^2]_s^{1/2}$) remain finite, showing the second-order transition from the noncollinear ferromagnetism (*F*) to the noncollinear SG.

The analyses of the single-site energy $E_0(\boldsymbol{\xi},z,i)$ and the pair energies $\Phi_{\alpha\pm}^{(e)}(\boldsymbol{\xi},z,i)$ $(\alpha=\mathbf{x},\mathbf{y},\mathbf{z})$ in Eq. (88), show that the SG region is further divided into two regimes according to the difference in the SG formation mechanism.

In the region $7.2 \lesssim N \lesssim 7.38$, the nearest-neighbor (NN) couplings are ferromagnetic and thus the local moments (LM's) form ferromagnetic clusters. However, there exist the long-range antiferromagnetic couplings which suppress the development of ferromagnetic long-range order, thus forming the SG accompanied by ferromagnetic clusters.

In the region $6.9 \lesssim N \lesssim 7.2$, the amorphous metals show anomalous magnetic couplings; the LM's with large amplitude ferromagnetically couple with the neighboring LM's, while the LM's with small amplitude antiferromagnetically

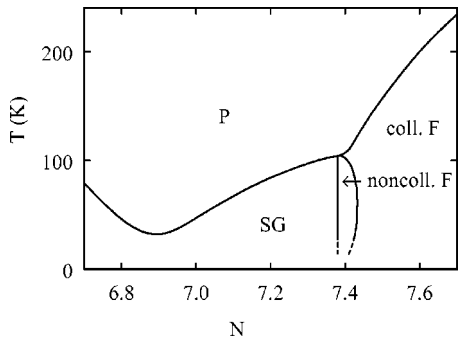

FIG. 3. Magnetic phase diagram as a function of temperature T and d electron number N, showing the paramagnetic, the collinear ferromagnetic (collinear F), the noncollinear ferromagnetic (noncollinear F), and the spin glass (SG) states.

couple with the neighboring ones. Since the amplitude of the LM depends strongly on the surrounding environment in this region, the sign of magnetic couplings changes with the local environment, thus leading to form the SG. It should be noted that the SG in amorphous Fe ($N \sim 7.0$) is caused by this mechanism.

The mechanisms shown here are essentially the same as those found for the SG in the collinear calculations.[14] Since the transverse spin degrees of freedom are taken into account in the present theory, the noncollinear SG is obtained in the present case. Figure 2(a) shows a LM distribution for the SG expected in amorphous Fe, where 4000 data points sampled from the 32 000 Monte Carlo data for $N=7.0$ and 30 K, are presented. It is seen that the LM distribution is nearly spherical. It should be noted that the distribution of LM's deviates from the spherical one in the vicinity of $N=6.9$, where the SG order parameter shows a minimum. In this region, the LM's show nearly two-dimensional disk shaped distribution [see Fig. 2(b)].

We have calculated the Curie temperature, the spin-glass transition temperature, and the transverse spin freezing temperature as functions of the d electron number. The obtained magnetic phase diagram is presented in Fig. 3. The phase diagram below 25 K was not calculated because of the numerical difficulty in calculations. The Curie temperature T_C rapidly decreases when the d electron number decreases and reaches the multicritical point at $N=7.38$ and $T=104$ K. The

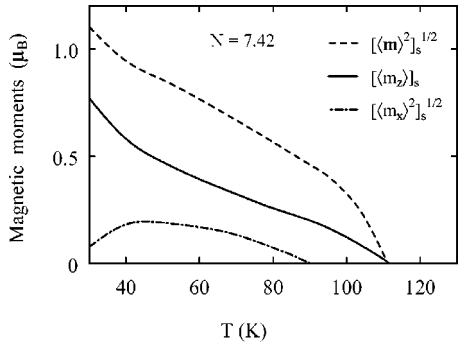

FIG. 4. Total spin-glass order parameter $[\langle \mathbf{m} \rangle^2]_s^{1/2}$, the magnetization $[\langle m_z \rangle]_s$, and the transverse spin-glass order parameter $[\langle m_x \rangle^2]_s^{1/2}$ as functions of temperature T for $N=7.42$.

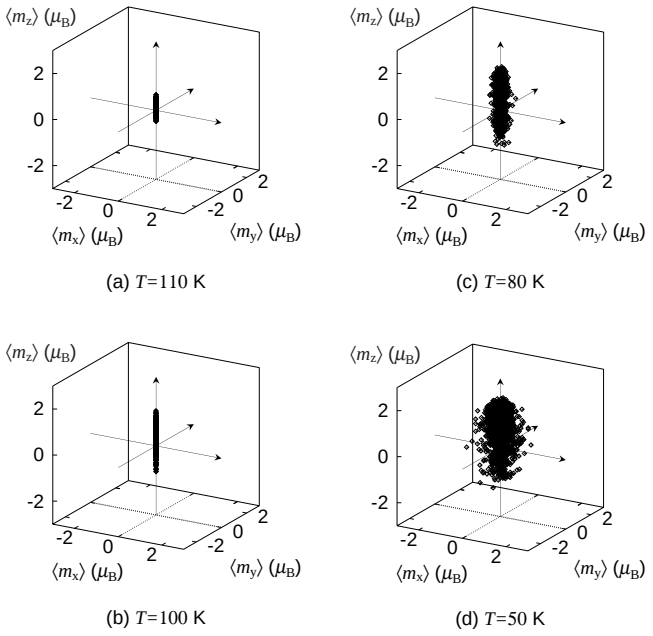

FIG. 5. The temperature dependence of the local moment distributions for $N=7.42$. Here 4000 data points among 32 000 Monte Carlo samplings are shown at temperatures (a) $T=110$ K, (b) $T=100$ K, (c) $T=80$ K, and (d) $T=50$ K. The magnetic polarization is assumed to be in the **z** direction.

SG transition temperature T_g shows a minimum as a function of N around $N=6.9$, where the average NN magnetic interactions change the sign. We have also calculated T_g for the collinear SG and have found that the T_g of the noncollinear SG is $1 \sim 3$ K higher than that of the collinear SG in the region $6.9 < N < 7.38$, while they are nearly the same in the region $N \lesssim 6.9$. This means that the noncollinear SG is expected in the region $6.9 \lesssim N \lesssim 7.38$, while the collinear and the noncollinear SG are almost degenerate for $N \lesssim 6.9$.

The transverse spin freezing temperature T_f is identified as a point where the transverse SG order parameter $[\langle m_x \rangle^2]_s^{1/2}$ appears. The curves of T_C and T_f in the vicinity of the multicritical point display two distinct transitions with decreasing temperature: the first to a collinear ferromagnetic state at T_C and the second to a noncollinear ferromagnetic state at T_f below T_C.

In order to see the details of the transverse spin freezing phenomenon, we show in Fig. 4 the curves of the magnetization $[\langle m_z \rangle]_s$, the total SG order parameter $[\langle \boldsymbol{m} \rangle^2]_s^{1/2}$, and their transverse component $[\langle m_x \rangle^2]_s^{1/2}$ $(=[\langle m_y \rangle^2]_s^{1/2})$ as functions of temperature for $N=7.42$. The magnetization curve shows that the spontaneous magnetization appears at 112 K. The transverse SG order parameters remain zero down to 90 K, showing the development of the collinear ferromagnetic order in the temperature range 90–112 K. Below 90 K, the transverse SG order parameter appears in the presence of finite magnetization. This result shows the appearance of the noncollinear F due to the freezing of transverse spin components. It is also seen that the transverse SG order parameter is reduced below 40 K. The extrapolation of the result to lower temperatures leads to the slight shrink of

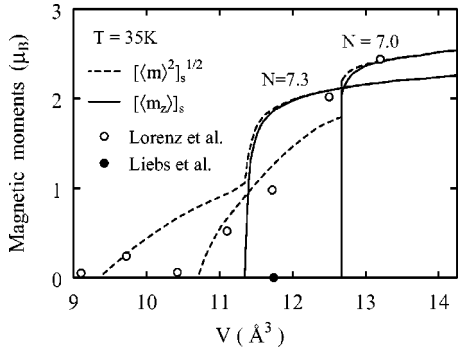

FIG. 6. Total spin-glass order parameter $[\langle \mathbf{m} \rangle^2]_s^{1/2}$ and the magnetization $[\langle m_z \rangle]_s$ as functions of volume for $N=7.0$ and 7.3 at 35 K. Calculated magnetization for amorphous Fe at the ground state by Lorenz and Hafner (Ref. 30) and that by Liebs *et al.* (Ref. 31) are presented by open and full circles, respectively.

the noncollinear ferromagnetic phase below 40 K, as seen in the magnetic phase diagram in Fig. 3.

Figure 5 shows the LM distribution corresponding to Fig. 4. The development of the collinear ferromagnetic order below T_C [Figs. 5(a) and 5(b)] and the subsequent development of the noncollinear ferromagnetic order below the transverse spin freezing temperature [Fig. 5(c) and 5(d)] are clearly seen. It should be noted that the LM's in Fig. 5 show a broad amplitude distribution even at 50 K. The feature is characteristic to the itinerant magnetism and is consistent with the recent Mössbauer measurements[8] in Fe-rich amorphous Fe-Zr alloys, which show broad internal field distributions at low temperatures.

In the experimental investigations on Fe-rich amorphous transition-metal alloys, the bulk magnetization,[5] Mössbauer,[8,32–34] and ac susceptibility[6] data, indicate two transitions for the alloys with less than 90 at. % Fe; the first to a collinear F state at T_C, and the second to a noncollinear state at a temperature below T_C due to the spin freezing. The proposed microscopic interpretations for the noncollinear phase, however, are not unique and are controversial even for the same alloy system.

Amorphous Fe-La alloys with more than 10 at. % La were reported to show a re-entrant F-SG transition below T_C, due to the freezing of transverse components of spins.[32] In the case of the amorphous Fe-Zr system, various microscopic models are proposed to describe the noncollinear phase below the spin freezing temperature. These include the freezing of frustrated antiferromagnetic clusters distributed in a ferromagnetic matrix (mictomagnetism),[6] the SG due to the freezing of ferromagnetic clusters with random orientations in a ferromagnetic matrix,[36] and the noncollinear ferromagnetism due to the homogeneous transverse spin freezing (asperomagnetism).[34] It was also reported that the noncollinear magnetic states in all the $Fe_{100-x}Zr_x$ ($7 \leqslant x \leqslant 12$), alloys become collinear under the external field of less than 7 T.[33] It has not been clarified, however, whether the observed noncollinear state is due to the atomic level of local canting for spins or it is due to the possible reorientations of larger collinear spins or domain structures.

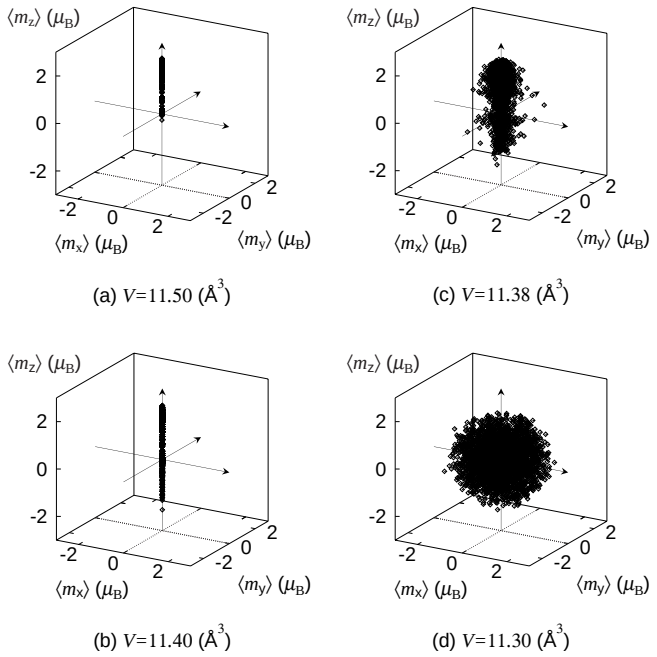

FIG. 7. The volume dependence of the local moment distributions at 35 K. Here 4000 data points among 32 000 Monte Carlo samplings are shown for the volumes (a) $V=11.50$ Å^3, (b) $V=11.40$ Å^3, (c) $V=11.38$ Å^3, and (d) $V=11.30$ Å^3. The magnetic polarization is assumed to be in the **z** direction.

The common feature among these results is that in the vicinity of the multicritical point ($\sim$90 at. % Fe), some kind of noncollinear state appears at a temperature below T_C due to the spin freezing, which seems to correspond to the present results shown in Figs. 4 and 5. It should be noted, however, that the experimental investigations mentioned above were performed at finite concentrations of the second elements, while the present calculations have been performed for amorphous pure transition metals by varying the d electron number. In general, the changing of the second element concentration is not the same as the changing of the d electron number, because the former brings about the additional effects of the alloying such as the random magnetic interactions and the atomic size effect due to the second element.[54] Therefore, the effects of the second element must be taken into account in the theory to clarify the observed spin freezing in Fe-rich amorphous alloys, which is left for future work.

B. Volume dependence

We have calculated the volume dependence of the magnetization and the SG order parameters for d electron numbers around amorphous Fe. We adopted the same input parameters as those used in the previous calculations.[22] The input DOS was scaled by the bandwidth $W \propto r^{-\kappa}$ ($\kappa=3.8$)[51,52] when the volume is changed. Here r denotes the Wigner-Seitz radius. The average coordination number z was chosen to be 12. The volume dependence of the effective exchange energy parameter $\tilde{J}$, was taken from the calculation by Andersen *et al.*[55] as follows:

$$\tilde{J}=\tilde{J}_0\left(-0.2\frac{r}{r_0}+1.2\right), \tag{98}$$

where $\tilde{J}_0=0.068$ Ry,[56] and $r_0=2.697$ a.u.[53] The fluctuation of interatomic distance is taken to be $[(\delta R)^2]_s^{1/2}/[R]_s=0.06$.

Figure 6 shows the volume dependence of the calculated magnetization $[\langle m_z\rangle]_s$ (solid curves), and the SG order parameter $[\langle \boldsymbol{m}\rangle^2]_s^{1/2}$ (dotted curves) for *d* electron numbers $N=7.0$ and 7.3 at 35 K. In the case of $N=7.0$ (corresponding to pure amorphous Fe), with decreasing volume, the magnetization suddenly drops at the critical volume 12.67 Å^3, where the first-order transition from the collinear *F* to the noncollinear SG takes place. Below 12.67 Å^3, the SG order parameter gradually decreases until the volume 10.70 Å^3, below which the paramagnetic state appears. The result agrees with that of the collinear calculations based on the finite-temperature theory of amorphous metallic magnetism,[22] where the first-order *F*-SG transition is shown to occur at the critical volume 12.55 Å^3 for $N=7.0$ at 75 K. Note that the noncollinear SG is obtained below the critical volume in the present theory with the transverse spin degrees of freedom.

It should also be noted that the obtained critical volume 12.67 Å^3 is close to the equilibrium volume 12.38 Å^3 [corresponding roughly to that of sputter-deposited amorphous Fe (Ref. 27)] of amorphous Fe. As discussed in Ref. 22, the ferromagnetism of amorphous Fe in the Y/Fe/Y layered structure[20] can be explained, provided that the volume of the amorphous Fe is expanded due to the presence of Y layers.

In the case of $N=7.3$, the magnetization continuously decreases with decreasing volume and disappears at the critical volume 11.3 Å^3, where the second-order transition to the noncollinear SG takes place. The noncollinear SG continues to exist until the volume 9.35 Å^3, below which a paramagnetic state appears. In the *F*-SG transition, the noncollinear *F* appears in a very narrow range of volume $11.30\,\text{Å}^3\leqslant V\leqslant 11.40\,\text{Å}^3$, as illustrated in the LM distributions in Fig. 7. It is seen that LM's antiparallel to the magnetization, appear first [Figs. 7(a) and (b)] and then the transverse components develop [Fig. 7(c)] with decreasing volume from 11.50 Å^3. Finally, a noncollinear SG with a nearly isotropic LM distribution is realized [Fig. 7(d)]. With regard to the noncollinear SG in the present paper, we remark that the distribution of LM's deviates from the spherical one in the vicinity of the boundary where the LM's disappear (e.g., $V\sim 9.4\,\text{Å}^3, N=7.3$ in Fig. 6). In this region, the LM's show a nearly two-dimensional disk shaped distribution as found in Fig. 2(b).

The volume dependence of the magnetism in amorphous Fe was also investigated on the basis of the ground-state theory. Lorenz and Hafner[30] performed detailed noncollinear calculations based on the self-consistent LMTO recursion method with 1728 atoms in a cluster. As shown in Fig. 6, their result shows a gradual decrease of magnetization down to 9.1 Å^3 with decreasing volume. It does not reveal a clear phase transition, although a SG-like state with noncollinear LM's is obtained below the volume 10.4 Å^3. It should be noted that there is no reason for the existence of the unique solution in the competing system such as amorphous Fe. In fact, Liebs *et al.*[31] performed noncollinear calculations with the use of the LMTO supercell method with 32 Fe atoms in a unit cell, and showed that the isotropic SG can become the ground state for $V=11.74\,\text{Å}^3$ (see Fig. 6). The *F*-SG phase transition is observed to occur in amorphous $Fe_{87.5}La_{12.5}$ alloys with increasing pressure.[42] The transition was found to be of second order. The nature of the volume-induced *F*-SG transition for pure amorphous Fe, however, has not been clarified experimentally.

IV. SUMMARY

We have developed the noncollinear theory of amorphous metallic magnetism on the basis of the functional-integral method and the distribution function method. The theory takes into account the transverse spin degrees of freedom at finite temperatures and reduces to the generalized Hartree-Fock approximation at the ground state. On the basis of the noncollinear theory, we have revealed the magnetic phase diagram of amorphous transition metals as a function of *d* electron number *N* and temperature *T*.

The obtained magnetic phase diagram on the *N*-*T* plane displays the spin-glass (SG) ($N\leqslant 7.38$), the noncollinear ferromagnetism (*F*) ($7.38\leqslant N\leqslant 7.43$), and the collinear *F* ($7.43\leqslant N$) at low temperatures. The noncollinear SG with nearly isotropic LM distribution is expected to be realized in the region $6.9<N\leqslant 7.38$. The Curie temperature T_C monotonically decreases with the decreasing *d* electron number *N*, and reaches the multicritical point at $N=7.38$. The spin-glass transition temperature T_g shows a minimum around $N=6.9$, where the average interactions change the sign. The *d* electron number dependence of T_C and T_g seems to be consistent with the recent experimental data on $Y_{20}(Mn_{1-x}Fe_x)_{80}$ quasibinary amorphous alloys,[57] in which the Curie temperature rapidly decreases until the SG state appears with the decreasing Fe concentration, and the SG transition temperature shows a minimum at $x=0.5$.

In the vicinity of the multicritical point on the *N*-*T* plane, the transition from the collinear *F* to the noncollinear *F* is shown to occur with decreasing temperature, due to the freezing of the transverse spin components. The result seems to be consistent with those of the recent Mössbauer measurements[8,32–34] on Fe-rich amorphous alloys. The LM distributions for the collinear *F* were found to remain broad due to the local environment effects even at low temperatures. This is characteristic of the itinerant electron system and agrees with the Mössbauer measurements on Fe-rich amorphous alloys, showing the broad internal field distributions at low temperatures.

We have also investigated the volume dependence of magnetism in amorphous transition metals for $N=7.0$ and 7.3 at 35 K. In both cases, the calculated magnetization versus volume curves show a phase transition from the *F* to the noncollinear SG and a subsequent transition to the paramagnetism with decreasing volume. The transition from the *F* to SG is shown to be of the first order for $N=7.0$, and to be of the second-order for $N=7.3$. The critical volume of the *F*-SG transition for $N=7.0$ is found to be close to the equilibrium volume of amorphous Fe, in agreement with the re-

sult of the collinear calculations.[22] The result can explain the observed ferromagnetism of amorphous Fe in a Y/Fe/Y layered structure, provided that the volume of the amorphous Fe is expanded due to the presence of Y layers.

Finally, we remark on the remaining problems in the theoretical treatments. First, in the present theory, the magnetic interactions between nearest-neighbor (NN) LM's are treated directly and the interactions with more distant LM's are taken into account as the effective media; the effects of the next NN interactions, for example, are not taken into account explicitly in the present treatment. The direct inclusion of the distant interactions may yield more delicate and detailed balance between the ferro- and the antiferromagnetic couplings. The effects may extend the region of the noncollinear ferromagnetism in the N-T phase diagram shown in Fig. 3, and may also change the nature of the transition from the F to SG with decreasing volume.

Second, the application of the present theory is limited to the magnetism of amorphous pure transition metals, while all the experimental data were obtained from the amorphous transition-metal alloys since it is not possible to realize the amorphous pure metals. Thus, in order to clarify the validity of the theory, it is necessary to extend the present theory to the case of amorphous alloys, taking into account the effects of the alloying such as the random magnetic interactions and the atomic size effects.[54] Such a theory would also explain the details of the experimental magnetic phase diagram in Fe-rich amorphous alloys.

ACKNOWLEDGMENTS

The authors would like to thank Professor K. Fukamichi, Professor K. V. Rao, Professor H. Tange, and Professor S. Murayama for valuable discussions. We are also indebted to Dr. M. Ohta for informing us of their experimental data on $Y_{20}(Mn_{1-x}Fe_x)_{80}$ quasibinary amorphous alloys. This work was done partly with use of the facilities of Hokkaido University Computing Center, the facilities of Data Processing Center, Kyoto University, and the Supercomputer Center in the Institute for Solid State Physics, The University of Tokyo.

[1] K. Moorjani and J.M.D. Coey, *Magnetic Glasses* (Elsevier, Amsterdam, 1984).
[2] P. Hansen, in *Handbook of Magnetic Materials*, edited by K.H. Bushow (North-Holland, Amsterdam, 1991), Vol. 6, p. 289.
[3] J.A. Fernandez-Baca and W.Y. Ching, *The Magnetism of Amorphous Metals and Alloys* (World Scientific, Singapore, 1995).
[4] K. Fukamichi, T. Goto, H. Komatsu, and H. Wakabayashi, in *Proceedings of the Fourth International Conference on the Physics of Magnetic Materials, Poland, 1988*, edited by W. Gorkowski, H.K. Lachowics, and H. Szymczak (World Scientific, Singapore, 1989), p. 354.
[5] H. Hiroyoshi and K. Fukamichi, Phys. Lett. A **85**, 242 (1981); J. Appl. Phys. **53**, 2226 (1982).
[6] N. Saito, H. Hiroyoshi, K. Fukamichi, and N. Nakagawa, J. Phys. F: Met. Phys. **16**, 911 (1986).
[7] J.M.D. Coey, D.H. Ryan, and R. Buder, Phys. Rev. Lett. **58**, 385 (1987).
[8] D.H. Ryan, J.M.D. Coey, E. Batalla, Z. Altounian, and J.O. Ström-Olsen, Phys. Rev. B **35**, 8630 (1987).
[9] H. Tange, Y. Tanaka, M. Goto, and K. Fukamichi, J. Magn. Magn. Mater. **81**, L243 (1989).
[10] J.A. Fernandez-Baca, J.J. Rhyne, G.E. Fish, M. Hennion, and B. Hennion, J. Appl. Phys. **67**, 5223 (1990).
[11] G.K. Nicolaides and K.V. Rao, J. Magn. Magn. Mater. **125**, 195 (1993).
[12] Y. Kakehashi, Phys. Rev. B **40**, 11 059 (1989).
[13] Y. Kakehashi, Phys. Rev. B **41**, 9207 (1990).
[14] Y. Kakehashi, Phys. Rev. B **43**, 10 820 (1991); **47**, 3185 (1993).
[15] J. Hubbard, Phys. Rev. B **19**, 2626 (1979); **20**, 4584 (1979); **23**, 597 (1981).
[16] H. Hasegawa, J. Phys. Soc. Jpn. **46**, 1504 (1979); **49**, 178 (1980).
[17] Y. Kakehashi, Phys. Rev. B **34**, 3243 (1986).
[18] F. Matsubara, Prog. Theor. Phys. **52**, 1124 (1974); S. Katsura, S. Fujiki, and S. Inawashiro, J. Phys. C **12**, 1839 (1979).
[19] M. Yu, Y. Kakehashi, and H. Tanaka, Phys. Rev. B **49**, 352 (1994).
[20] S. Handschuh, J. Landes, U. Köbler, Ch. Sauer, G. Kisters, A. Fuss, and W. Zinn, J. Magn. Magn. Mater. **119**, 254 (1993).
[21] R. Bellissent, G. Galli, N.W. Grinstaff, P. Migliardo, and K.S. Suslick, Phys. Rev. B **48**, 15 797 (1993).
[22] M. Yu and Y. Kakehashi, Phys. Rev. B **49**, 15 723 (1994).
[23] Y. Kakehashi, T. Uchida, and M. Yu, Phys. Rev. B **56**, 8807 (1997).
[24] H. Al-Attar and Y. Kakehashi, J. Appl. Phys. **86**, 3265 (1999).
[25] S. Krompiewski, U. Krauss, and U. Krey, Phys. Rev. B **39**, 2819 (1989).
[26] W.Y. Ching and Y.N. Xu, J. Appl. Phys. **70**, 6305 (1991).
[27] I. Turek and J. Hafner, Phys. Rev. B **46**, 247 (1992).
[28] A.M. Bratkovsky and A.V. Smirnov, Phys. Rev. B **48**, 9606 (1993); J. Phys.: Condens. Matter **5**, 3203 (1993).
[29] U. Krey, U. Krauss, and S. Krompiewski, J. Magn. Magn. Mater. **103**, 37 (1992).
[30] R. Lorenz and J. Hafner, J. Magn. Magn. Mater. **139**, 209 (1995).
[31] M. Liebs, K. Hummler, and M. Fähnle, Phys. Rev. B **51**, 8664 (1995).
[32] H. Wakabayashi, T. Goto, K. Fukamichi, H. Komatsu, S. Morimoto, and A. Ito, J. Phys. Soc. Jpn. **58**, 3383 (1989).
[33] I. Vincze, D. Kaptás, T. Kemény, L.F. Kiss, and J. Balogh, Phys. Rev. Lett. **73**, 496 (1994).
[34] H. Ren and D.H. Ryan, Phys. Rev. B **51**, 15 885 (1995).
[35] R.A. Cowley, N. Cowlam, P.K. Ivison, and J. Martinez, J. Magn. Magn. Mater. **104-107**, 157 (1992).
[36] S.N. Kaul and Ch.V. Mohan, J. Appl. Phys. **71**, 6090 (1992); **71**, 6103 (1992).
[37] M. Gabay and G. Toulouse, Phys. Rev. Lett. **47**, 201 (1981).
[38] J.R. Thomson, H. Guo, D.H. Ryan, M.J. Zuckermann, and M. Grant, Phys. Rev. B **45**, 3129 (1992).

[39] T. Uchida and Y. Kakehashi, J. Appl. Phys. **81**, 3859 (1997); Physica B **239**, 504 (1997).
[40] T. Uchida and Y. Kakehashi, J. Magn. Magn. Mater. **177-181**, 83 (1998).
[41] T. Uchida and Y. Kakehashi, J. Appl. Phys. **87**, 7139 (2000).
[42] T. Goto, C. Murayama, N. Mori, H. Wakabayashi, K. Fukamichi, and H. Komatsu, J. Phys. (Paris), Colloq. **49**, C8-1143 (1988).
[43] J. Hubbard, Phys. Rev. Lett. **3**, 77 (1959).
[44] R.L. Stratonovich, and Dokl. Akad. Nauk SSSR **115**, 1097 (1958) [Sov. Phys. Dokl. **2**, 416 (1958)].
[45] H. Hasegawa, J. Phys. F: Met. Phys. **13**, 1915 (1983).
[46] Y. Kakehashi, Phys. Rev. B **35**, 4973 (1989).
[47] R. Yamamoto and M. Doyama, J. Phys. F: Met. Phys. **9**, 617 (1979).
[48] M. Matsuura, H. Wakabayashi, T. Goto, H. Komatsu, and K. Fukamichi, J. Phys.: Condens. Matter **1**, 2077 (1989).
[49] P. Soven, Phys. Rev. **156**, 809 (1967); B. Velicky, S. Kirkpatrick, and H. Ehrenreich, *ibid.* **175**, 747 (1968).
[50] H. Miwa, Prog. Theor. Phys. **52**, 1 (1974).
[51] V. Heine, Phys. Rev. **153**, 673 (1967).
[52] U.K. Poulsen, J. Kollár, and O.K. Andersen, J. Phys. F: Met. Phys. **6**, L241 (1976).
[53] T. Fujiwara, Nippon Butsuri Gakkaishi **40**, 209 (1985).
[54] M. Yu and Y. Kakehashi, J. Phys.: Condens. Matter **8**, 5071 (1996).
[55] O.K. Andersen, J. Madsen, U.K. Poulsen, O. Jepsen, and J. Kollár, Physica B **86-88**, 249 (1977).
[56] J.F. Janak, Phys. Rev. B **16**, 255 (1977).
[57] M. Ohta, A. Fujita, K. Fukamichi, Y. Obi, and H. Fujimori, J. Phys.: Condens. Matter **11**, 4053 (1999).